

In-plane bending of Timoshenko beams in bilateral frictionless contact with an elastic half-space using a coupled FE-BIE method

Daniele BARALDI^a, Nerio TULLINI^b

^a corresponding author; DACC - Department of Architecture, Construction, Conservation;

Università IUAV di Venezia, Italy; e-mail: danielebaraldi@iuav.it

^b Department of Engineering; University of Ferrara, Italy; e-mail: nerio.tullini@unife.it

ABSTRACT

Making use of a mixed variational formulation including the Green function of the substrate, a finite element model is derived for the static analysis of Timoshenko beams in bilateral frictionless contact with an elastic half-space. Numerical results are obtained by adopting locking-free Hermite polynomials for the Timoshenko beam and piecewise constant reaction over the soil. Foundation beams loaded by forces and couples at the midspan illustrate accuracy and convergence properties of the proposed formulation.

Keywords: Soil-structure interaction; Frictionless bilateral contact; Mixed variational principle; Boussinesq solution; Timoshenko beam; Locking-free finite element.

1. INTRODUCTION

In this paper, static analyses of beams on a three-dimensional (3D), elastic and isotropic half-space are considered. Strip footing adopted in building structures is a typical example of beam resting on a half-space. For this reason, static analyses of beams resting on half-space or soil were performed by many researchers up to present days and a wide range of analytical and numerical models can be found in literature [1-9], characterized by different assumptions for foundation elements and for half-space behavior.

Focusing on 3D half-space behavior, the early studies of Boussinesq and Cerruti [10, 11] defined the Green functions of an elastic and isotropic 3D half-space. Starting from such Green functions, the expressions for stresses and displacements generated by a vertical force applied on the half-space surface can be determined. Analyses related to the determination of displacements generated by various force distributions on the surface of the half-space were carried out by many researchers [1, 4, 6, 8, 9]. For instance, Love [12] determined surface displacements generated by a uniform pressure over a rectangular area, whereas the indentation of a rigid punch on a half-space represents another problem which involves Boussinesq solution [10, 11].

The static analysis of beams on 3D half-space was considered for the first time by Biot [13], who studied an Euler-Bernoulli (E-B) beam having infinite length resting on an elastic half-space adopting Fourier integrals. Beam deflection was considered only along its longitudinal axis and a relation between half-space elastic parameters and the Winkler subgrade constant was suggested. The same problem was studied by Rvachev [14], that also extended the solution to a strip in flexure along both contact surface directions [15]. Lekkerkerker [16] proposed an asymptotic solution of the integral equation arising from the general differential equation of the beam on half-space, whereas the corresponding rigorous solution was obtained by Koiter [17, 18]. Gorbunov-Possadov [19] studied E-B beams having infinite and finite length on elastic half-space adopting the power series method. Barden [20] studied E-B beams of finite length on elastic half-space adopting power series

and compared the results with experimental data. Then, Vesic [21] solved the same problem introduced by Biot and considered the case of an infinite beam loaded by a concentrated load and a couple. More recent developments dealing with infinite beams are represented by the contributions of Selvadurai and co-workers, that studied an infinite beam embedded in an elastic half-space [22] and resting on a poroelastic half-space [23].

In order to numerically solve interaction problems of beams and plates resting on elastic foundation, both Finite Element (FE) and Boundary Element (BE) methods were largely adopted by many authors [7]. Finite element method (FEM) allows to describe complex soil media and surface profiles [4, 24]. However, the substrate mesh has to be extended far away from the loaded area to ensure vanishing displacements at the boundaries, leading to a huge number of FEs. To improve the computational efficiency, infinite elements were used, see [7, 25] and references cited therein. It is worth observing that using classical beam FEs and brick FEs for the substrate does not allow for the angular continuity at the contact surface. In principle, this problem may be solved by introducing special interface elements between brick and plate bending elements [26].

In the boundary element method (BEM), only the boundary of the substrate has to be meshed. In this field, an important contribution was given, among the others, by Brebbia, Katsikadelis, Banerjee and their co-workers, that introduced BEM both for generic elastic domains [27-30] and for plates on Winkler-type support [31, 32]. BEM was applied to a wide variety of engineering problems up to present days [33], including soil-structure-interaction problems, see [34, 35] and references cited therein. However, soil tractions are usually considered as nodal reactions in the FE model of the raft and the rotation continuity between beam and substrate is neglected. In the general formulation of BEM dealing with elastic half-space, Mindlin's fundamental solution was usually adopted to obtain the displacement field due to a point force applied in the interior of a homogeneous three-dimensional elastic solid [36]. The particular problem discussed in the present paper refers to loads applied to the ground surface of a half-space. Consequently, Boussinesq solution [10, 11] is the proper fundamental solution to be used. In this framework, the first

satisfactory solution for a square raft of arbitrary flexibility resting on an elastic foundation was obtained by Cheung and Zienkiewicz [37]. Cheung and Nag [38] used a similar technique to account for horizontal contact pressures beneath the raft. In these methods, the raft was modeled by rectangular plate elements where the uniform soil reactions were lumped at the FE nodes and the flexibility matrix of the half-space was obtained by using the Boussinesq fundamental solution. Consequently, this approach required the explicit inversion of the substrate flexibility matrix. Moreover, a pinned-clamped rigid link connecting the plate element to the substrate was implicitly assumed. Thus, no angular continuity between plate and substrate could be imposed. Variational formulations including the Green function of the substrate were first presented in [39-41] and in the contributions of Selvadurai dedicated to plates on elastic half-space [42, 43], also accounting for plate shear deformability [44-46]. In [47], the analysis of frames with rigid footings resting on an isotropic elastic half-space is reported. In [48, 49], the static analysis of Timoshenko beam on elastic multilayered soils by combination of finite element and analytical layer element was analysed. Solution to multilayered soils under axisymmetric loading was used, so introducing some errors in substrate traction modeling. Moreover, adequate soil traction distribution in beam transverse direction was neglected.

With reference to elastic half-plane, the static analysis of Timoshenko beams and frames in frictionless [50, 51] or fully adhesive [52, 53] contact with an half-plane was analysed by means of a Finite Element-Boundary Integral Equation (FE-BIE) method. An analogous study concerning bars and thin coatings can be found in [54], and in [55] accounting for debonding. Moreover, the FE-BIE coupling method was also used to study the buckling of Euler-Bernoulli [56] and Timoshenko [57] beams in bilateral frictionless contact with an elastic half-plane. The numerical performance of the abovementioned FE-BIE coupling method shown an excellent convergence rate in comparison with those of other standard numerical methods.

In this paper, the coupled FE-BIE method introduced in [50] is extended to study the in-plane bending of Timoshenko beams in bilateral frictionless contact with an elastic, isotropic half-space.

The assumption of beam deflections varying only along x direction requires uniform displacements along y direction. In particular, the mixed variational formulation assumes as independent fields both the surface tractions and the beam displacements and rotations, whereas existing variational formulations for beams and plates on half-space usually assume displacements as unknowns of the problem. The numerical model makes use of locking-free “modified” Hermitian shape functions [58-61] for the beam and piecewise constant function for the substrate tractions.

Differently from the majority of the methods available in the literature, see for example [4, 37, 38], the adopted coupled FE-BIE method enforces the angular continuity between the foundation beam and the half-space surface at the node locations. Moreover, the proposed model involves symmetric substrate matrices, whereas the classical FEM-BEM approach based on collocation BEM requires an additional computational effort to remedy the lack of symmetry of the BEM coefficient matrix. If the ground surface underneath the foundation beam is meshed with rectangular elements, the weakly singular BIE is evaluated analytically, so avoiding singular behavior in the numerical evaluation of the integrals, that are the major concern of the classical BEM [62]. Furthermore, soil traction distribution in beam transverse direction can be considered adopting an adequate FE mesh refinement of contact surface. Finally, the resolving matrix has dimensions proportional to the number of the foundation beam FEs. Vice versa, in the standard FEM, a refined mesh requires a stiffness matrix with dimensions that are several times the square of the number of FEs used for the foundation beam. The advantages outlined result in accurate solutions at low computational cost. To the authors’ knowledge, the present proposal to use the coupled FE-BIE model for the static analysis of shear deformable beams in bilateral frictionless contact with an elastic 3D half-space represents a new contribution.

A variety of numerical examples is presented to show the effectiveness of the proposed model. An initial convergence test is performed in order to evaluate the influence of the accuracy of contact surface discretization on the behavior of a foundation beam subject to a vertical point force at midspan, with particular attention to the discretization along the beam width. This case study is

adopted for a further convergence test that compares the results of the proposed model with respect to a classical 3D FEM. Furthermore, several parametric examples are performed, accounting for varying half-space stiffness and beam length to cross-section width ratio, and evaluating the influence of shear deformations typical of Timoshenko beams. Results are compared with existing analytical and numerical solutions, showing the effectiveness of the model in representing the behavior of a foundation beam resting on a 3D half-space with small computational effort.

2. VARIATIONAL FORMULATION

A foundation beam, with length L , resting in bilateral frictionless contact with a semi-infinite substrate, is referred to a Cartesian coordinate system $(0; x, y, z)$, where the x - y plane defines the boundary of the half-space and x coincides with the centroidal axis of the beam, whereas z is chosen in the downward transverse direction. Beam cross-section shape is assumed to be symmetric about the axis z , with height h and width b representing the overall cross-section dimensions in z and y direction. Moreover, a flat cross-section base is considered, in order to define a contact area between the beam and the half-space as a strip of constant width b and length L . A distributed vertical external load $p(x)$ and a distributed external couple $m(x)$ are applied in the plane of symmetry along the beam axis x (Fig. 1), allowing the beam to experience flexure only in x - z plane. On the interface between beam and substrate, frictionless and bilateral conditions are assumed, so that only a vertical half-space traction $r(x, y)$ is acting upon the beam. The beam is made of homogeneous linearly elastic material, with longitudinal and transverse elastic moduli E_b , G_b , and Poisson coefficient ν_b . The isotropic material of the substrate is characterized by the elastic modulus E_s and by the Poisson ratio ν_s . Focusing on the half-space behavior, the vertical displacement w of a point on its boundary due to a generic surface traction $r(\hat{x}, \hat{y})$ is given by the Boussinesq solution [10, 11]:

$$w(x, y, 0) = \frac{(1-\nu_s^2)}{\pi E_s} \int_{-b/2}^{b/2} \int_L \frac{r(\hat{x}, \hat{y}) d\hat{x} d\hat{y}}{d(x, y; \hat{x}, \hat{y})}, \quad (1)$$

where

$$d(x, y; \hat{x}, \hat{y}) = \sqrt{(x - \hat{x})^2 + (y - \hat{y})^2} \quad (2)$$

is the distance between the points $(x, y, 0)$ and $(\hat{x}, \hat{y}, 0)$. Due to the theorem of work and energy for exterior domains [63], the strain energy of the soil is

$$U_s = \frac{1}{2} \int_{-b/2}^{b/2} \int_L r(x, y) w(x, y, 0) dx dy, \quad (3)$$

and, therefore, the potential energy of the soil Π_s can be written as

$$\Pi_s = U_s - \int_{-b/2}^{b/2} \int_L r(x, y) w(x, y, 0) dx dy = -\frac{1}{2} \int_{-b/2}^{b/2} \int_L r(x, y) w(x, y, 0) dx dy. \quad (4)$$

Substituting Eq. (1) into Eq. (4) yields

$$\Pi_s = -\frac{(1-\nu_s^2)}{2\pi E_s} \int_{-b/2}^{b/2} \int_L r(x, y) dx dy \int_{-b/2}^{b/2} \int_L \frac{r(\hat{x}, \hat{y}) d\hat{x} d\hat{y}}{d(x, y; \hat{x}, \hat{y})}. \quad (5)$$

Assuming positive cross-section rotation φ in counterclockwise direction and restricting the analysis in the x - z plane, axial and transverse displacements of a Timoshenko beam with symmetric cross-section can be written as:

$$u(x, y, z) = \varphi(x) z, \quad v(x, y, z) = 0, \quad w(x, y, z) = w(x). \quad (6a, b, c)$$

The corresponding nonzero axial and shear strains become:

$$\varepsilon = \varphi' y, \quad \gamma = w' + \varphi, \quad (7)$$

where prime represents differentiation with respect to x . Stress-strain relations yield:

$$\sigma = E_b \varepsilon, \quad \tau = G_b \gamma. \quad (8)$$

Using strain components (7) and constitutive laws (8), the elastic strain energy for the in-plane bending of a beam of length L can be written in the form:

$$U_b = \frac{1}{2} \int_L [E_b J_b \varphi'^2 + k_b G_b A_b (w' + \varphi)^2] dx, \quad (9)$$

where A_b and J_b are the cross-sectional area and the second moment of area with respect to the y axis, respectively, and k_b is the shear factor [64]. The potential energy Π_b of the beam can be written as

$$\Pi_b = U_b - \int_L \left[\left(p(x) - \int_{-b/2}^{b/2} r(x, y) dy \right) w(x) + m(x) \varphi(x) \right] dx. \quad (10)$$

Hence, making use of Eqs. (5) and (10), the total potential energy of the beam-substrate system turns out to be

$$\Pi(w, \varphi, r) = \Pi_b(w, \varphi, r) + \Pi_s(r). \quad (11)$$

Variational formulation analogous to Eq. (11) was obtained in [39, 41] for beams resting on a Pasternak soil and in [50, 51] for beams and frames resting in bilateral frictionless contact with an elastic half-plane. Moreover, mixed variational principle similar to Eq. (11) was used in [54] to study axially loaded thin structures perfectly bonded to an elastic substrate and in [56, 57] to determine the buckling loads of beams in frictionless contact with an elastic half-plane. Beams in perfect adhesion with an elastic half-plane are considered in [52, 53]. Differently with respect the proposed approach, traditional variational formulations are defined in terms of foundation displacements only [42-46].

It is worth noting that the beam model hypothesis implies vertical displacement w varying only along x direction, see Eq. (6c), and uniform vertical displacement along beam width. Focusing on the behavior of the model along the beam width, two limit cases may be defined: uniform vertical

displacement and uniform contact traction. A uniform contact traction distribution in y direction produces a transverse deflection and the beam cannot be considered with a rigid cross-section (Fig. 2a). Vice versa, a uniform displacement along beam width is obtained if the beam cross-section is infinitely rigid with respect to the half-space in the y direction, then the distribution of contact stresses in the transverse direction is expected to be equal to the one generated by a rigid indenter with width b in a plane strain problem [10, 11] (Fig. 2b). The effect of changing the distribution of the soil pressure in the y direction was investigated in [13], where it is shown that the ratio of average loads and deflections varies only about 10% when the distribution of soil pressure changes from a uniform one to one giving constant vertical displacement across the width b . It is worth noting that different transverse soil distribution yields alternative Green function [39]. The assumption of beam deflections varying only along x direction implies an infinite beam section stiffness along y direction, leading to uniform displacements along y direction; in the next section, different subdivision methods of the beam-substrate contact interface are investigated in order to evaluate their influence on the resulting beam displacement and contact stress distribution.

3. DISCRETE MODEL

Dividing the beam into n_x FEs having length l_{xi} (see Fig. 3 for the case of equal beam FEs), the displacement field for the i th element can be approximated in the usual form:

$$\mathbf{d}_i(\xi) = \mathbf{N}(\xi) \mathbf{q}_i \quad (12)$$

where $\xi = x/l_{xi}$, $\mathbf{d}(\xi) = [w(\xi), \varphi(\xi)]^T$ collects the two displacement functions, $\mathbf{q}_i = [w_1, \varphi_1, w_2, \varphi_2]^T$ denotes the vector of nodal displacements and the matrix $\mathbf{N}(\xi)$ assembles the following “modified” shape functions N_{1j} and N_{2j} ($j = 1, \dots, 4$) [58, 59, 60, 61]:

$$N_{11} = \left[1 - 3\xi^2 + 2\xi^3 + \phi_i(1-\xi) \right] / (1 + \phi_i), \quad N_{12} = -l_{xi} \xi \left[(1-\xi)^2 + \phi_i(1-\xi)/2 \right] / (1 + \phi_i), \quad (13a, b)$$

$$N_{13} = [3\xi^2 - 2\xi^3 + \phi_i \xi] / (1 + \phi_i), \quad N_{14} = -l_{xi} \xi [-\xi + \xi^2 - \phi_i(1 - \xi)/2] / (1 + \phi_i), \quad (13c, d)$$

$$N_{21} = 6\xi(1 - \xi) / [l_{xi}(1 + \phi_i)], \quad N_{22} = [1 - 4\xi + 3\xi^2 + \phi_i(1 - \xi)] / (1 + \phi_i), \quad (13e, f)$$

$$N_{23} = -6\xi(1 - \xi) / [l_{xi}(1 + \phi_i)], \quad N_{24} = (-2\xi + 3\xi^2 + \phi_i \xi) / (1 + \phi_i). \quad (13g, h)$$

These “modified” shape functions depend on a coefficient ϕ_i that takes the expression:

$$\phi_i = \frac{12E_b J_b}{k_b G_b A_b l_{xi}^2} \quad (14)$$

that accounts for the shear deformation according to the Timoshenko beam theory. As shown in [59], the finite element interpolation functions (13) give exact nodal displacements as they derive from the exact solution of the homogeneous governing equations for a Timoshenko beam. Moreover, Eqs. (13) reduce to the classical Hermitian polynomials (and to their derivatives) when shear deformations are negligible, so resulting in locking-free FEs [59, 61].

The contact surface underneath the beam may be divided in x and y directions by means of different methods, then $n_x \cdot n_y$ surface elements having length l_{xi} and width l_{yi} are defined, leading to a total number of $n_x(n_y + 2) + 2$ unknowns of the entire soil-structure system, represented by beam degrees of freedom and half-space surface tractions. Surface subdivisions in x direction are assumed to be coincident with those of the foundation beam, whereas subdivisions in y direction, i.e. across the beam width, are needed for modelling the non-uniform pressures generated by uniform displacements. The simplest surface subdivision method is the regular one with $l_{xi} = L/n_x$ and $l_{yi} = b/n_y$. However, it is well known that a rigid punch as well as the problem at hand exhibits a singular behavior near the edges and corners of the rectangular surface [4, 10, 11]. Therefore, a regular mesh should be very refined to describe correctly displacements and reactions at contact surface edges and corners. In order to obtain accurate results with a small number of surface subdivisions, it is common to use power graded meshes [65, 66], which are characterized by a grading exponent $\beta \geq$

1. In particular, an interval $[-0.5, 0.5]$ subdivided in n points is described by the following coordinates:

$$t_j = \begin{cases} \frac{1}{2} \left[\left(\frac{2j}{n} \right)^\beta - 1 \right] & \text{for } 0 \leq j \leq n/2 \\ -t_{n-j} & \text{for } n/2 < j \leq n \end{cases} \quad (15)$$

For $\beta = 1$ the subdivision turns out to be uniform, but as β increases, the elements near the ends of the interval tend to be smaller and smaller, whereas the elements close to the origin tend to be larger.

In the following, as previously stated, the length of a generic surface element along the beam length (x direction) is assumed equal to the beam FE length l_{xi} , and vice versa. However, in order to evaluate correctly the soil pressure singularities near the beam extremities, a power-graded mesh with a number of subdivisions $n_{x,end}$ is also introduced for the sub-elements at the beam ends, leading to $n_{x,tot} = n_x - 2 + 2n_{x,end}$ subdivisions along the x direction. Considering then the possible subdivisions along the beam width (y direction), one subdivision requires uniform half-space reactions along the y direction, but such a traction distribution corresponds to a foundation beam with a deformable cross-section with respect to the half-space (Fig. 2a), contradicting the assumed hypothesis of rigid cross-section. Vice versa, more subdivisions along beam width allow to describe the surface traction singularities close to the beam section ends (Fig. 2b). Nonetheless, the behavior of a beam with a rigid cross-section with respect to the half-space can be achieved only with an infinite number of subdivisions.

Fig. 4 shows some examples of contact surface subdivisions. Starting from the simple case of a beam with $n_x = 8$, $n_{x,end} = 1$ and $n_y = 1$ corresponding to an uniform mesh, the second and third row show discretizations characterized by $n_y = 3$ and 5, respectively. Such discretizations are obtained by using the power graded function along the y axis (Eq. 15) with $\beta = 3$ and $n = 4$ and 6, respectively, and merging the subdivisions adjacent to the midpoint. Second and third column show

discretizations characterized by $n_{x,end} = 2$ and 3, respectively. In the numerical examples presented in the following section, analyses are carried out by increasing the number of subdivisions n_x along longitudinal direction and considering the nine combinations presented in Fig. 4.

The k th soil surface FE underlying the beam is characterized by a length l_{xj} and width l_{yj} , with $k = (j-1)n_x + i$ and i, j varying from 1 to $n_{x,tot}$ and n_y , respectively. Accordingly, the soil reaction can be approximated as

$$r_k(\xi, \eta) = [\boldsymbol{\rho}(\xi, \eta)]^T \mathbf{r}_k, \quad (16)$$

where $\eta = y/l_{yj}$, \mathbf{r}_k denotes the vectors of nodal soil reaction and $\boldsymbol{\rho}(\xi, \eta)$ assembles the substrate shape functions. In the following, constant shape functions $\boldsymbol{\rho}(\xi, \eta)$ are assumed; thus, only one soil traction is defined over a contact surface element and a constant piecewise traction distribution is assumed underneath the beam.

Substituting Eqs. (12, 16) in variational principal (11) and assembling over all the elements, the potential energy takes the expression

$$\Pi(\mathbf{q}, \mathbf{r}) = \frac{1}{2} \mathbf{q}^T \mathbf{K}_b \mathbf{q} - \mathbf{q}^T \mathbf{F} + \mathbf{q}^T \mathbf{H} \mathbf{r} - \frac{1}{2} \mathbf{r}^T \mathbf{G} \mathbf{r}, \quad (17)$$

where \mathbf{K}_b is the stiffness matrix of the beam and \mathbf{F} the external load vector, whose components for the generic element are as usual

$$k_{b,ij} = \frac{1}{l_{xi}} \int_0^1 D_b(\xi) \left[N'_{2i}(\xi) N'_{2j}(\xi) + \frac{12}{\phi_i} \left(\frac{1}{l_{xi}} N'_{1i}(\xi) + N_{2i}(\xi) \right) \left(\frac{1}{l_{xi}} N'_{1j}(\xi) + N_{2j}(\xi) \right) \right] d\xi, \quad (18)$$

$$f_i = b l_{xi} \int_0^1 N_{1i}(\xi) p_z(\xi) + N_{2i}(\xi) m(\xi) d\xi, \quad (19)$$

whereas the components of matrices \mathbf{H} and \mathbf{G} are

$$h_{ij} = l_{xi} l_{yj} \int_0^1 N_{li}(\xi) d\xi \int_0^1 \rho_j(\xi, \eta) d\eta, \quad (20)$$

$$g_{ij} = \frac{(1-\nu_s^2)}{\pi E_s} \int_{y_i}^{y_{i+1}} \int_{x_i}^{x_{i+1}} \rho_i(x, y) dx dy \int_{\hat{y}_j}^{\hat{y}_{j+1}} \int_{\hat{x}_j}^{\hat{x}_{j+1}} \frac{\rho_j(\hat{x}, \hat{y}) d\hat{x} d\hat{y}}{d(x, y; \hat{x}, \hat{y})}, \quad (21)$$

where $(x_i, x_{i+1}; y_i, y_{i+1})$ are the (global) coordinates of the i th surface FE and $(\hat{x}_i, \hat{x}_{i+1}; \hat{y}_i, \hat{y}_{i+1})$ are the coordinates of the j th surface FE. The matrices appearing in Eq. (17) are reported in Appendix. It is worth noting that the matrix \mathbf{G} , which may be defined as the flexibility matrix of the half-space, is fully populated since it takes into account the nonlocal relation between beam deflection and contact traction. Moreover, the integral in Eq. (21) is weakly singular, i.e., it always exists and is finite.

Requiring the potential energy to be stationary, the following system of equations is obtained

$$\begin{bmatrix} \mathbf{K}_b & \mathbf{H} \\ \mathbf{H}^T & -\mathbf{G} \end{bmatrix} \begin{Bmatrix} \mathbf{q} \\ \mathbf{r} \end{Bmatrix} = \begin{Bmatrix} \mathbf{F} \\ \mathbf{0} \end{Bmatrix}, \quad (22)$$

whose formal solution gives

$$\mathbf{r} = \mathbf{G}^{-1} \mathbf{H}^T \mathbf{q}, \quad (23)$$

$$(\mathbf{K}_b + \mathbf{K}_{\text{soil}}) \mathbf{q} = \mathbf{F}, \quad (24)$$

where \mathbf{K}_{soil} is the stiffness matrix of the soil or 3D half-space

$$\mathbf{K}_{\text{soil}} = \mathbf{H} \mathbf{G}^{-1} \mathbf{H}^T \quad (25)$$

and Eq. (24) represents the discrete system of equations governing the response of the soil-structure system.

It is worth noting that the second row of Eq. (22) includes beam displacements and rotations due to half-space tractions and matrix \mathbf{H} plays a key role in enforcing the displacement compatibility between beam and half-space surface. Furthermore, the validity of Eq. (23) does not depend on the

presence of a foundation beam, but it may be used for determining the surface tractions generated by a generic displacement field \mathbf{q} assigned to the half-plane boundary.

4. NUMERICAL EXAMPLES

According to references [4, 13, 21], the parameter characterizing the soil-foundation system is

$$\alpha L = \sqrt[3]{\frac{E_s b L^3}{(1-\nu_s^2) D_b}}. \quad (26)$$

Low values of αL characterize short beams stiffer than the soil, when the beams perform like a rigid punch. Large values of αL describe more flexible beams, thus are appropriate for long beams on stiff soil. In the following, symbol E is used instead of $E_s/(1-\nu_s^2)$. Moreover, the parameter $\chi = L/b$ have to be defined in order to complete the description of the beam geometry; for instance, long beams are characterized by large values of χ . Parameters αL and χ are typically adopted for studying beams resting on half-space [4, 20]. Making use of Eq. (14), shear deformation is characterized by the parameter

$$\phi = \frac{12D_b}{kG_b AL^2}. \quad (27)$$

For isotropic beam with $\nu_b = 0.2$ and slenderness L/h equal to 3, 5 or 10, the coefficient ϕ is approximately equal to 0.3, 0.1, 0.03, respectively.

In this section, static analyses of beams with free ends and finite length resting in bilateral frictionless contact with an elastic half-space are dealt with. Three simple load cases are considered: vertical point force at midspan, uniform vertical load distribution along the beam length and couple at midspan.

It is worth noting that the half-space behavior is linear and bilateral. Consequently, tractions along contact surface may result both tensile (negative values) and compressive (positive values).

However, considering more complex load conditions and, in particular, adding the effects of the self-weight of the foundation, surface tractions turn out usually to be compressive.

For the sake of simplicity, beams with rectangular cross-sections are assumed having $\nu_b = 0.2$ and coefficient $\phi = 0.3$. The Euler-Bernoulli beam case ($\phi = 0$) is also considered.

4.1. Beam loaded by a vertical point force at midspan

4.1.1 – Influence of contact surface discretization

In this section, a foundation beam resting on an elastic half-space loaded by a vertical point force P_z at midspan is considered. The first example refers to an Euler-Bernoulli beam having $\chi = 10$, subdivided with $n_x = 2^8$ FEs, $n_{x,end} = 1$ and by considering three cases of subdivision along y direction: $n_y = 1$, $n_y = 3$ and 5 adopting a power-graded mesh with $\beta = 3$. Figs. 5a, b show dimensionless beam displacement $w/[P_z/(Eb)]$ for $\alpha L = 5$ and 25 , respectively. Displacements obtained with $n_y = 3$ and $n_y = 5$ appear almost coincident, whereas with $n_y = 1$ beam displacement is slightly larger than the other results. Similar considerations can be done about dimensionless surface tractions $r(x, 0)/[P_z/(Lb)]$ along the beam length (Fig. 5c, d). Tractions obtained with one subdivision along y direction are larger with respect to the other cases, whereas tractions obtained with $n_y = 3$ and $n_y = 5$ are quite close to each other. Moreover, Figs. 6a, b show surface tractions at midspan along the beam width. It is worth noting that $n_y = 1$ corresponds to the case of a flexible beam cross-section that cannot be correctly represented by a beam model; the corresponding uniform traction along beam width at midspan is smaller than minimum tractions obtained with $n_y = 3$ and 5 . On the other hand, 3 or 5 graded subdivisions along y direction are able to model traction singularities near edges, but only a large number of subdivisions allows to obtain the actual traction distribution along beam width typical of a rigid indenter in plane strain conditions.

Convergence tests are performed in order to evaluate the influence of the number of subdivisions n_y along beam width on the overall system behavior for increasing regular longitudinal subdivisions n_x . For this purpose, a numerical reference solution in terms of displacements w^{REF} and tractions

r^{REF} , obtained with a refined beam and contact surface discretization, is assumed. In particular, for the reference solution $n_x = 2^{10}$, $n_{x,\text{end}} = 3$ and a power-graded subdivision along y direction with $n_y = 7$ and $\beta = 3$ are adopted. Reference results are collected in Tab. 1. Fig. 7 shows relative differences $\delta_{w(0)} = [w(0) - w^{\text{REF}}(0)]/w^{\text{REF}}(0)$ and $\delta_{r(0)} = [r(0,0) - r^{\text{REF}}(0,0)]/r^{\text{REF}}(0,0)$ versus n_x for $\alpha L = 5, 25$ and $n_y = 1, 3, 5$. The adopted subdivisions along y direction influence significantly the results, with relative differences tending to constant values instead of tending to zero. If only one subdivision is adopted along beam width, differences are larger than those obtained with 3 and 5 subdivisions. In particular, differences for beam displacement at midpoint are close to 3% and 4% for $\alpha L = 5$ and 25, respectively, whereas differences for the traction at midpoint are close to 45% and 30%, showing that one subdivision along beam width does not allow to obtain accurate results. Adopting three power graded subdivisions along beam width, relative differences are smaller with respect to the previous case, in particular they are close to 0.4% and 0.6% for beam displacement at midpoint for $\alpha L = 5$ and 25, respectively, whereas differences for traction at midpoint are close to 10% and 7% for $\alpha L = 5$ and 25, respectively. Finally, five power graded subdivisions along beam width give differences close to 0.1% for beam displacement at midpoint and both αL cases, whereas traction at midpoint is characterized by differences close to 2% for both αL cases. These convergence tests show that half-space reactions strictly depend on contact surface discretization and differences with respect to reference solutions are larger than those obtained for beam displacements, which are less influenced by contact surface discretization. Moreover, differences generally decrease for increasing half-space stiffness. Considering discretization along beam length and focusing on the results obtained with power graded meshes, it must be pointed out that the differences with respect to reference results start to converge to the values previously depicted when n_x is close to 2^6 , except for the displacements evaluated with $\alpha L = 5$.

Considering the results of this convergence tests, the following examples will consider contact surface discretization with $n_y = 3$ and will avoid further discretization at beam ends by assuming $n_{x,\text{end}} = 1$.

4.1.2 – Comparison with a 3D FEM

In this section, another convergence test is performed by comparing the proposed model with respect to a classical 3D FEM of a beam on elastic half-space loaded by a vertical force at midspan. For this purpose, the half-space is modelled by a cubic mesh having an overall size equal to $4L$, composed of non-uniform cubic and rectangular prismatic brick elements, whereas the foundation beam is modelled as an Euler-Bernoulli beam subdivided into equal FEs. In the 3D mesh, horizontal displacements normal to the vertical edges are fixed, together with vertical and horizontal displacements fixed at the base of the model. The mesh is refined close to the foundation beam and it is coarse close to the boundaries. The mesh refinement is adopted in order to correctly represent the contact surface between the foundation beam and the half-space in x and y directions. Focusing on the contact surface, equal subdivisions along both directions are adopted and brick element size in x direction is equal to beam FE length. The frictionless connection between beam and half-space is established by vertical master-slave links, which connect each beam node to the contact surface nodes having the same x coordinate, allowing to obtain a uniform vertical displacement along contact surface width. The 3D FEM is refined up to 2^6 beam FEs; however, in order to reduce the computational effort of the convergence test, only one quarter of the 3D FEM is actually modelled, and Fig. 8 shows the case of the foundation beam subdivided into 4 beam FEs.

Considering a beam with $\chi = 10$ subject to a vertical force at midspan, with $n_x = 2^6$, results in terms of dimensionless displacements $w/[P_z/(Eb)]$ and tractions $r(x, 0)/[P_z/(Lb)]$ obtained with the 3D FEM are added to Fig. 5 with solid circles, whereas Fig. 9 a, b shows results in terms of dimensionless bending moment $M/(P_z L)$ obtained with the 3D FEM (solid circles) and with the proposed model with $n_y = 3$ (continuous lines). The 3D FEM turns out to be less deformable and characterized by small surface tractions with respect to the proposed model, especially in case of stiff foundation beam on soft soil; whereas results in terms of bending moment are in excellent agreement with those of the proposed model.

Assuming the numerical reference solutions of the previous section in terms of displacements and tractions at midpoint, Fig. 7 collects also relative differences versus n_x obtained with the 3D FEM (line with solid circles), for $\alpha L = 5$ and 25. The displacements at midpoint obtained with the 3D FEM converge very slowly to reference solutions, with differences close to 8%, whereas the corresponding tractions at midpoint better converge to the results of the proposed model with $n_y = 3$, even if differences with respect to reference solutions are close to 11% for $\alpha L = 5$ and close to 20% for $\alpha L = 25$. Focusing then on bending moment at midspan, Fig. 9 c, d shows differences with respect to reference solution $\delta_{M(0)} = [M(0) - M^{\text{REF}}(0)]/M^{\text{REF}}(0)$ versus the overall number of degrees of freedom of each model. In this case, both the 3D FEM and the proposed model converge rapidly to reference solutions, with differences close to 4% for the 3D FEM and close to 0.3% for the proposed model. It is worth noting that Fig. 9 shows that the overall number of degrees of freedom of the 3D FEM, even if related to one quarter of the entire 3D model, is several orders of magnitude larger than that of the proposed model with $n_y = 3$.

This convergence test showed that a classical 3D FEM may require a more refined discretization and a larger computational effort with respect to the proposed model, especially in terms of beam displacements and contact tractions.

Then, considering the results of both convergence tests, in order to have sufficiently accurate results but also to limit the overall number of unknowns of the upcoming numerical tests, the following examples adopt $n_x = 2^8$, $n_{x,end} = 1$ and $n_y = 3$.

4.1.2 – Parametric tests

Several analyses are carried out for different values of the parameter αL . Figs. 10 and 11 show dimensionless displacement $w/[P_z/(Eb)]$, dimensionless half-space traction $r/[P_z/(Lb)]$ and dimensionless bending moment $M/(P_z L)$ versus x/L , for values of the parameter αL equal to 1, 5, 10, 100, which correspond to beams of increasing length on stiff soil. Each figure show results for ϕ equal to 0 and 0.3.

Fig. 10a shows dimensionless vertical displacements referred to $\alpha L = 1$, in this case the mean displacement is larger than the maximum relative displacement; thus the beam behaves like a rigid rectangular indenter. Moreover, for $\phi = 0.3$, a wedge-shaped beam deflection is obtained. Figs. 10c, e show that both surface tractions and bending moments do not depend significantly on ϕ . Moreover, surface tractions are characterized by a singular behavior at beam ends, typical of a rectangular rigid punch.

Results obtained with $\alpha L = 5$ are shown in Figs. 10b, d, f. In this case the mean displacement is smaller than the maximum relative displacement (Fig. 10b) and, for $\phi = 0.3$, a wedge-shaped beam deflection generates singular half-space tractions at midpoint (Fig. 10d). Bending moment values decrease for increasing the value of ϕ (Fig. 10f).

Figs. 11a, c, e show results obtained with $\alpha L = 10$, which turn out to be quite similar to those obtained with $\alpha L = 5$. Fig. 11b, d, f is referred to $\alpha L = 100$. For $\phi = 0.3$, the system of equations (22) tends to be singular, then the corresponding results are not shown. It is worth noting that the vertical displacement shown in Fig. 11b is well approximated by Boussinesq solution (1) that reduces to

$$w(x,0) = \frac{P_z}{\pi E} \frac{1}{|x|}, \quad (28)$$

as shown with cross symbols in Fig. 11b, except in the neighbourhood of the point load, where Euler-Bernoulli beam enforces the continuity of w' in the surface displacements.

Fig. 12a shows dimensionless displacement at beam midpoint and beam end versus αL . For very low αL values, both displacements tend to be coincident with those given by a rigid punch. For instance, such displacements are both close to $\bar{w} = 0.21 P_z / (Eb)$, leading to a translational stiffness of the system $k_w = P_z / \bar{w} = 0.48 EL$, that is in excellent agreement with data determined by Whitman and Richart [67] for $\chi = 10$. Increasing αL , displacement at midpoint obviously increases, whereas displacement at beam ends converges to a constant value given by Eq. (28) for $x = L/2$:

$$w(L/2) = \frac{P_z}{\pi E L} \frac{2}{L} \Rightarrow \frac{w(L/2)}{P_z/(Eb)} = \frac{2}{\pi \chi} \quad (29a, b)$$

which is equal to 0.064 for $\chi = 10$ irrespective of the shear deformation parameter ϕ .

Fig. 12b shows dimensionless traction $r(L/2 - 2L/n_x, 0)$ close to the beam end versus αL . For a beam on stiff soil, tractions assume large values due to the singular behavior showed in Fig. 10c. For $\alpha L > 3$ tensile tractions close to the beam ends are obtained and, for increasing αL , tractions tend to zero. In fact, the singular behavior at the ends of slender beams on stiff soil is restricted to a zone with length lesser than $2l_x = 2L/2^8$.

Biot [13] studied the behavior of an infinite Euler-Bernoulli beam resting on an elastic half-space loaded by a concentrated force P_z , the maximum bending moment is expressed by:

$$M(0) = 0.166 P_z b \left[16 k \frac{D_b}{Eb^4} \right]^{0.277} = 0.166 \frac{P_z L}{\chi} \left[16 k \left(\frac{\chi}{\alpha L} \right)^3 \right]^{0.277}, \quad (30)$$

where k is a parameter introduced by Biot and set equal to 1 in the case of uniform pressure distribution along the beam width and equal to 1.13 in the case of uniform deflection along the beam width. The present model, characterized by tractions varying in both x and y direction ($n_y = 3$), follows sufficiently the hypothesis of uniform deflection along the beam width. Then, setting χ equal to 10, 30 and 100, the bending moment $M(0)$ is evaluated for increasing αL values and compared to Eq. (30) assuming $k = 1.13$. Fig. 13 shows that Eq. (30), represented with dashed lines, is in good agreement with the results of the present analysis for $\alpha L > 3$. Therefore, Eq. (30) can be profitably used for beam of finite length.

4.2. Beam loaded by an uniform force distribution

In this section, a foundation beam resting on an elastic half-space loaded by a uniform force distribution p along its entire length is considered. The examples refer to a beam with $\chi = 10$, $n_x = 2^8$, $n_{x,end} = 1$ and $n_y = 3$ adopting a power-graded mesh.

For $\alpha L = 1$, Fig. 14a shows that beam displacements are characterized by a rigid body vertical translation and a small deflection. Surface tractions presented in Fig. 14c are typical of a rigid indenter. Moreover, surface traction and bending moment are not influenced by ϕ . For $\alpha L = 5$, surface tractions (Fig. 14d) are characterized by singularities at beam ends. Both displacement (Fig. 14b) and tractions are not influenced by ϕ , whereas bending moment (Fig. 14f) decreases as ϕ increases. Displacements and tractions obtained with $\alpha L = 10$ (Fig. 15a, c) are quite similar to those obtained with $\alpha L = 5$, whereas bending moment (Fig. 15e) is quite different and characterized by large values close to $x = \pm L/4$. For $\alpha L = 100$, the results are presented only for the Euler-Bernoulli beam case (Figs. 15b, d, f) due to the singular behavior of matrix in Eq. (22). Beam displacements (Fig. 15b) are quite different to those determined with Love analytic solution (Eq. 3.25 in [10]), which are shown with cross symbols in the figure. Surface tractions (Fig. 15d) are nearly constant along the beam length excluding singularities at the beam ends, whereas bending moment (Fig. 15f) is characterized by two peaks close to the beam ends.

Fig. 16a shows dimensionless displacement at midpoint and beam end versus αL . For beam on stiff soil, both displacements tend to be coincident with those corresponding to a rigid punch. In fact, starting from the almost uniform displacement $\bar{w} = 2.12 p/E$ for $\alpha L = 1$, the translational stiffness turns out to be $k_w = pL/\bar{w} = 0.47 EL$, that is again in agreement with existing data [67] and it is quite close to the value obtained in the previous case study. Increasing αL , displacement at midspan tend to converge to a constant value close to $2.4 p/E$, which is smaller than $2.51 p/E = 0.8 \pi p/E$ that is the solution of a rectangular loaded area having $L/b = 10$ (Eq. 3.25 in [10]), whereas displacement at beam ends is quite close to the analytic solution $1.48 p/E = 0.47 \pi p/E$. Fig. 16b shows dimensionless tractions at beam midpoint versus αL , starting from $0.63 p/b$, that corresponds to the value that may be obtained with a rigid rectangular punch [67]. It is worth noting that the pressures distribution underneath a slender beam on a stiff soil converge to a uniformly loaded area only if $n_y = 1$ is assumed (large dashed line in Fig. 16b). Vice versa, surface discretization along the beam width provides foundation rigidity in y direction. For this reason, dimensionless tractions for

$n_y = 3$ converge to a value close to $0.7 q_z/b$, that is less than a unitary uniform pressure p/b . Therefore, the case of uniform force distribution turns out to be more influenced by contact surface discretization across beam width with respect to the previous one.

4.3. Beam loaded by a couple at midspan

The case of a foundation beam loaded by a counterclockwise couple C at midspan is finally considered. The examples refer to a beam with $\chi = 10$, $n_x = 2^8$, $n_{x,end} = 1$ and $n_y = 3$ adopting a power-graded mesh. Figs. 17a, c, e show results relative to $\alpha L = 1$ in terms of dimensionless displacement, traction and bending moment. In this case results do not depend appreciably on ϕ . Beam displacement shows a rigid body rotation, whereas surface tractions present singularities near beam ends. Starting from absolute displacement at beam ends, rigid rotation $\theta = 1.55 C/[EL^2b]$ and the corresponding rotational stiffness of the system $k_\theta = C/\theta = 0.65 EL^2b$ is in agreement with existing data for a rigid rectangular indenter with $L/b = 10$ [67].

Figs. 17b, d, f show results for $\alpha L = 5$. In this case, maximum absolute displacements are attained close to $x = \pm L/4$, with larger absolute values obtained with $\phi = 0$, whereas tractions and bending moment are less influenced by ϕ . For $\alpha L = 10$, Figs. 18a, c, e show results quite different with respect to the previous cases, since they are more depending on ϕ . In particular, beam displacements and surface tractions with $\phi = 0.3$ are smaller than those obtained with the Euler-Bernoulli beam, moreover, maximum absolute values are obtained close to $x = \pm L/10$. For $\alpha L = 100$, Figs. 18b, d, f show results obtained with $\phi = 0$. In this case, the displacements, tractions and bending moment are concentrated close to beam midspan; then, a large number of subdivisions along x axis is necessary in order to obtain accurate results.

CONCLUSIONS

In this paper, static analyses of Timoshenko beams with finite length in frictionless and bilateral contact with an elastic and isotropic 3D half-space are presented. For this purpose, a simple and effective coupled finite element-boundary integral equation method, already adopted by the authors for static and buckling analysis of beams and frames on elastic half-plane, is extended to the more complex case of beams on 3D elastic half-space, that, for instance, is able to represent the behavior of shallow foundation beams. Starting from the Boussinesq solution of the displacement generated by a normal point force acting on the half-space surface, the boundary integral equation method is adopted by discretizing only contact surface pressures by means of a piecewise constant function. Beam stiffness matrix is determined by adopting locking free FEs based on “modified” Hermitian shape functions accounting for beam shear deformability. Several numerical tests are performed by considering beams of finite length subject to a concentrated vertical force, a concentrated couple and to a distributed vertical force. The proposed model turns out to be simple and effective in representing foundation behavior. In particular, for increasing beam stiffness, the behavior of the foundation converges to that of a flat rectangular punch and to the corresponding existing solutions in terms of punch translational and rotational stiffness. On the other hand, for increasing soil stiffness and, at the same time, for increasing beam slenderness, the behavior of the foundation converges to existing solutions for Euler-Bernoulli beams.

The proposed model turns out to be strictly dependent on the contact surface discretization along beam width, in particular considering results in terms of contact surface tractions. Assuming vertical displacements along beam width to be uniform, corresponding to the hypothesis of rigid beam cross-section, the distribution of contact tractions along beam width must follow the one typical of a rigid punch in plane strain conditions, characterized by singularities close to section ends. Such a traction distribution is obtained by subdividing contact surface along beam width too, in particular by adopting a power-graded mesh characterized by smaller and smaller subdivisions

close to section ends. A first convergence test limited to the case of a foundation beam loaded by a vertical force at midspan showed that the simplest case of contact surface mesh without subdivisions along the beam width turns out to be still sufficiently accurate in determining displacements, but extremely inaccurate in determining contact tractions, whereas three graded subdivisions along the beam width may be sufficient for obtaining accurate results in terms of both displacements and tractions. A second convergence test has been performed for comparing the proposed model with respect to a standard 3D FEM of an Euler-Bernoulli beam on half-space. This test showed an excellent agreement between the models in terms of beam bending moments, and a sufficient agreement in terms of beam displacements and contact tractions, due to the huge computational effort required by the 3D FEM.

Further developments of this work will regard for first the study of 3D framed structures with their shallow foundations resting on a half-space, in order to account for soil deformability on structural behavior. Then, further analyses will assume unilateral contact between the beam and the half-space, requiring to develop iterative techniques for identifying possible separation zones along the contact surface. The effect of adhesion and/or friction between the foundation beam and the half-space will be also taken into account, following the approach already adopted in [52-55].

ACKNOWLEDGMENTS

The present investigation was developed in the framework of the Research Program FAR 2017 of the University of Ferrara. Moreover, the analyses were developed within the activities of the (Italian) University Network of Seismic Engineering Laboratories–ReLUIS in the research program funded by the (Italian) National Civil Protection – Progetto Esecutivo 2014-2018 – Research Line “Reinforced Concrete Structures”. The financial support of the MIUR PRIN Projects 2015LYYXA8 and 2015JW9NJT is gratefully acknowledged.

APPENDIX

For a prismatic beam element subjected to uniform loads $p(x)$ and $m(x)$, element matrices \mathbf{K}_{bi} and \mathbf{F}_i become

$$\mathbf{K}_{bi} = \frac{D_b}{1 + \phi_i} \begin{bmatrix} 12/l_{xi}^3 & -6/l_{xi}^2 & -12/l_{xi}^3 & -6/l_{xi}^2 \\ & (4 + \phi_i)/l_{xi} & 6/l_{xi}^2 & (2 - \phi_i)/l_{xi} \\ & & 12/l_{xi}^3 & 6/l_{xi}^2 \\ \text{sym} & & & (4 + \phi_i)/l_{xi} \end{bmatrix},$$

$$\mathbf{F}_i = p [l_{xi}/2, -l_{xi}^2/12, l_{xi}/2, l_{xi}^2/12]^T + m/(1 + \phi_i) [1, l_{xi}\phi_i/2, -1, l_{xi}\phi_i/2]^T.$$

Considering n_y subdivisions along the beam width, the matrix \mathbf{H} for the generic i th beam element is given by the following expression:

$$\mathbf{H}_i^{ny} = \begin{bmatrix} l_{xi}/2 \\ -l_{xi}^2/12 \\ l_{xi}/2 \\ l_{xi}^2/12 \end{bmatrix} [l_{y1}, l_{y2}, \dots, l_{ny}]$$

For one subdivision ($n_y = 1$) along the beam width, the matrix \mathbf{H} for the generic i th beam element reduces to:

$$\mathbf{H}_i = b [l_{xi}/2, -l_{xi}^2/12, l_{xi}/2, l_{xi}^2/12]^T,$$

Considering the half-space surface subdivided into rectangular elements and adopting a piecewise constant substrate reaction, the components of the flexibility matrix \mathbf{G} of the half-space are:

$$g_{ij} = \frac{(1 - \nu_s^2)}{\pi E_s} \int_{y_i}^{y_{i+1}} \int_{x_i}^{x_{i+1}} dx dy \int_{\hat{y}_j}^{\hat{y}_{j+1}} \int_{\hat{x}_j}^{\hat{x}_{j+1}} \frac{d \hat{x} d \hat{y}}{d(x, y; \hat{x}, \hat{y})}$$

where the distance $d(x, y; \hat{x}, \hat{y})$ between the points $(x, y, 0)$ and $(\hat{x}, \hat{y}, 0)$ is reported in Eq. (2). The solution of the quadruple integral on a generic subdivision is:

$$g_{ij} = \frac{(1 - \nu_s^2)}{\pi E_s} \left[\left[\left[\left[F(x, y; \hat{x}, \hat{y}) \right]_{\hat{x}_j}^{\hat{x}_{j+1}} \right]_{\hat{y}_j}^{\hat{y}_{j+1}} \right]_{x_i}^{x_{i+1}} \right]_{y_i}^{y_{i+1}}$$

$$\begin{aligned}
&= \frac{(1-\nu_s^2)}{\pi E_s} \left[F(x_i, y; \hat{x}_j, \hat{y}) - F(x_i, y; \hat{x}_{j+1}, \hat{y}) - F(x_{i+1}, y; \hat{x}_j, \hat{y}) + F(x_{i+1}, y; \hat{x}_{j+1}, \hat{y}) \right]_{\hat{y}_j}^{\hat{y}_{j+1}} \Big|_{y_i}^{y_{i+1}} = \\
&= \frac{(1-\nu_s^2)}{\pi E_s} \left\{ F(x_i, y_i; \hat{x}_j, \hat{y}_j) - F(x_i, y_i; \hat{x}_{j+1}, \hat{y}_j) - F(x_{i+1}, y_i; \hat{x}_j, \hat{y}_j) + F(x_{i+1}, y_i; \hat{x}_{j+1}, \hat{y}_j) \right. \\
&\quad - \left[F(x_i, y_{i+1}; \hat{x}_j, \hat{y}_j) - F(x_i, y_{i+1}; \hat{x}_{j+1}, \hat{y}_j) - F(x_{i+1}, y_{i+1}; \hat{x}_j, \hat{y}_j) + F(x_{i+1}, y_{i+1}; \hat{x}_{j+1}, \hat{y}_j) \right] \\
&\quad - \left[F(x_i, y_i; \hat{x}_j, \hat{y}_{j+1}) - F(x_i, y_i; \hat{x}_{j+1}, \hat{y}_{j+1}) - F(x_{i+1}, y_i; \hat{x}_j, \hat{y}_{j+1}) + F(x_{i+1}, y_i; \hat{x}_{j+1}, \hat{y}_{j+1}) \right] \\
&\quad \left. + F(x_i, y_{i+1}; \hat{x}_j, \hat{y}_{j+1}) - F(x_i, y_{i+1}; \hat{x}_{j+1}, \hat{y}_{j+1}) - F(x_{i+1}, y_{i+1}; \hat{x}_j, \hat{y}_{j+1}) + F(x_{i+1}, y_{i+1}; \hat{x}_{j+1}, \hat{y}_{j+1}) \right\}
\end{aligned}$$

where $F(x, \hat{x}) = F_0(x, \hat{x}) + F_1(x, \hat{x})$ and

$$F_0(x, y; \hat{x}, \hat{y}) = -\frac{[d(x, y; \hat{x}, \hat{y})]^3}{6}$$

$$F_1(x, y; \hat{x}, \hat{y}) = \frac{1}{4} |x - \hat{x}| |y - \hat{y}| \left[|y - \hat{y}| \ln \frac{d + |x - \hat{x}|}{d - |x - \hat{x}|} + |x - \hat{x}| \ln \frac{d + |y - \hat{y}|}{d - |y - \hat{y}|} \right] \quad \text{for } x \neq \hat{x}, y \neq \hat{y}$$

$$F_1(x, x; y, \hat{y}) = F_1(x, \hat{x}; y, y) = 0$$

In particular

$$\begin{aligned}
g_{ii} = \frac{(1-\nu_s^2)}{\pi E_s} \left\{ -\frac{2}{3} [(l_{xi}^2 + l_{yi}^2)^{3/2} - (l_{xi}^3 + l_{yi}^3)] + \right. \\
\left. + l_{xi} l_{yi} \left[l_{yi} \ln \frac{(l_{xi}^2 + l_{yi}^2)^{1/2} + l_{xi}}{(l_{xi}^2 + l_{yi}^2)^{1/2} - l_{xi}} + l_{xi} \ln \frac{(l_{xi}^2 + l_{yi}^2)^{1/2} + l_{yi}}{(l_{xi}^2 + l_{yi}^2)^{1/2} - l_{yi}} \right] \right\}
\end{aligned}$$

REFERENCES

- [1] Poulos HG, Davis EH. Elastic solutions for soil and rocks mechanics. New York: John Wiley & Sons; 1974.
- [2] Hetenyi M. Beams on Elastic Foundations, Michigan: University of Michigan Press; 1976.
- [3] Desai CS, Christian JT. Numerical Methods in Geotechnical Engineering, New York: McGraw Hill; 1976.
- [4] Selvadurai APS. Elastic analysis of soil-foundation interaction. Developments in Geotechnical Engineering, Amsterdam: Elsevier; 1979.
- [5] Gladwell GML. Contact Problems in the Classical Theory of Elasticity, xxxx: Springer, 1980.
- [6] Hemsley JA. Elastic analysis of raft foundations. London: Thomas Telford; 1998.
- [7] Wang YH, Tham LG, Cheung YK. Beams and plates on elastic foundations: a review. Prog Struct Eng Mater 2005; 7(4):174-182.
- [8] Melerski ES. Design analysis of beams, circular plates and cylindrical tanks on elastic foundations. 2nd Ed. London: Taylor and Francis; 2006.
- [9] Tsudi E. Analysis of structures on elastic foundations. Plantation, FL: J. Ross Publishing; 2013.
- [10] Johnson KL. Contact mechanics. Cambridge: Cambridge University Press; 1985.
- [11] Kachanov ML, Shafiro B, Tsukrov I. Handbook of elasticity solutions. Dordrecht: Kluwer Academic Publishers; 2003.
- [12] Love AEH. The Stress Produced in a Semi-Infinite Solid by Pressure on Part of the Boundary. Philos Trans R Soc London. 1929; 228(659-669):377-420.
- [13] Biot MA. Bending of an infinite beam on an elastic foundation. J Appl Mech 1937; 4:A1–A7.
- [14] Rvachev VL. On the bending of an infinite beam on elastic half-space. J Appl Math Mech 1958; 22(5):984-988.

- [15] Protsenko VS, Rvachev VL. Plate in the form of an infinite strip on an elastic half-space. *J Appl Math Mech* 1976; 40(2):273-280.
- [16] Lekkerkerker JG. Bending of an infinite beam resting on an elastic half-space. *Proc K Ned Akad Wet Ser B*. 1960; 63:484-497.
- [17] Koiter WT. Approximate solution of Wiener-Hopf type integral equations with applications, *Proc K Ned Akad Wet Ser B*. 1954; 57:575-579.
- [18] Koiter WT. Solutions of some elasticity problems by asymptotic methods. *Proc IUTAM Symp Appl Theory Func*, Tblisi, 1963. Moscow, Nauka Publ House, 1965; 1:15-31.
- [19] Gorbunov-Posadov MI, Serebrjanyi RV. Design of structures on elastic foundations. *Proceedings 5th International Conference in Soil Mechanics and Foundation Engineering*. 1961; 1:643-648.
- [20] Barden L. Distribution of contact pressure under foundations. *Géotechnique* 1963; 12:181–188.
- [21] Vesic AB. Bending of beams on isotropic elastic medium. *J Eng Mech Div - ASCE* 1961; 87(EM2):35-53.
- [22] Selvadurai APS. The flexure of an infinite strip of finite width embedded in an isotropic elastic medium of infinite extent. *Int J Num Anal Meth Geomech* 1984; 8:157-166.
- [23] Selvadurai APS, Shi JL. Biot's problem for a Biot material. *Int J Eng Sci* 2015; 97:133-147.
- [24] Bathe KJ. *Finite element procedures*. Prentice Hall; 1996, 2nd ed. K.J. Bathe, Watertown, MA; 2014 and Higher Education Press, China; 2016.
- [25] Viladkar MN, Godbole PN, Noorzaei J. Space frame-raft-soil interaction including effect of slab stiffness. *Comput Struct* 1992; 43(1):93-106.
- [26] Kohnehpooshi O, Noorzaei J, Jaafar MS, Raizal Saifulnaz MR. Development of a special interface element between brick and plate bending elements. *Procedia Eng* 2011; 14:734-742.
- [27] Brebbia CA, Dominguez J. *Boundary Element Method for Potential Problems*. *Appl Math Model* 1977; 1:372-378.

- [28] Katsikadelis JT, Massalas CV, Tzivanidis GJ. An integral equation of the plane problem of the theory of elasticity. *Mech Res Comm* 1977; 4(3):199-208.
- [29] Brebbia, CA. *The Boundary Element Method for Engineers*. London: Pentech Press, 1978.
- [30] Banerjee, PK, Butterfield R. *Boundary Element Methods in Engineering Science*. New York: McGraw-Hill, 1981.
- [31] Katsikadelis, JT. *The analysis of plates on elastic foundation by the boundary element method*. Ph.D. dissertation. Polytechnic University of New York. 1982.
- [32] Costa JA, Brebbia C. The boundary element method applied to plates on elastic foundations. *Eng Anal* 1985; 2(4):174-183.
- [33] Katsikadelis JT. *Boundary Elements: Theory and Applications*. Oxford: Elsevier. 2002.
- [34] Beskos DE. *Boundary Element Methods in Geomechanics*. In: *Boundary Elements X*, Vol. 4 (ed. Brebbia CA.) 1988:3-28.
- [35] Ribeiro DB, Paiva JB. An alternative BE–FE formulation for a raft resting on a finite soil layer. *Eng Anal Bound Elem* 2015; 50:352–359.
- [36] Aleynikov S. *Spatial Contact Problems in Geotechnics. Boundary-Element Method*. Berlin Heidelberg: Springer-Verlag; 2011.
- [37] Cheung YK, Zienkiewicz OC. Plates and tanks on elastic foundations - an application of finite element method. *Int J Solids Struct* 1965; 1(4):451–461.
- [38] Cheung YK, Nag DK. Plates and beams on elastic foundation - linear and non-linear behaviour. *Geotechnique* 1968; 18(2):250–260.
- [39] Kikuchi N. Beam bending problems on a Pasternak foundation using reciprocal variational-inequalities. *Q Appl Math* 1980; 38(1):91-108.
- [40] Kikuchi N, Oden J. *Contact problems in elasticity. A study of variational inequalities and finite element methods*. Philadelphia: SIAM; 1988.
- [41] Bielak J, Stephan E. A modified Galerkin procedure for bending of beams on elastic foundations. *SIAM J Sci Stat Comput* 1983; 4(2):340–352.

- [42] Selvadurai APS. The Interaction between a Uniformly Loaded Circular Plate and an Isotropic Elastic Halfspace: A Variational Approach. *J Struct Mech* 1979; 7(3):231-246.
- [43] Selvadurai APS. Elastic contact between a flexible circular plate and a transversely isotropic elastic halfspace. *Int J Solid Struct* 1980; 16:167-176.
- [44] Selvadurai APS. A contact problem for a Reissner plate and an isotropic elastic halfspace. *J Mech Theor Appl* 1984; 3(2):181-196.
- [45] Rajapakse RKND, Selvadurai APS. On the performance of Mindlin plate elements in modelling plate-elastic medium interaction: a comparative study. *Int J Numer Methods Eng* 1986; 23:1229-1244.
- [46] Selvadurai APS, Dumont NA. Mindlin's Problem for a Halfspace Indented by a Flexible Plate. *J Elast* 2011; 105:253-269.
- [47] Guarracino F, Minutolo V, Nunziante L. A simple analysis of soil-structure interaction by BEM-FEM coupling. *Eng Anal Bound Elem* 1992; 10(4):283-289.
- [48] Ai ZY, Cai JB. Static analysis of Timoshenko beam on elastic multilayered soils by combination of finite element and analytical layer element. *Appl Math Model* 2015; 39(7):1875-1888.
- [49] Ai ZY, Cai JB. Static interaction analysis between a Timoshenko beam and layered soils by analytical layer element/boundary element method coupling. *Appl Math Model* 2016; 40(21-22):9485-9499.
- [50] Tullini N, Tralli A. Static analysis of Timoshenko beam resting on elastic half-plane based on the coupling of locking-free finite elements and boundary integral. *Comput Mech* 2010; 45(2-3):211-225.
- [51] Baraldi D, Tullini N. Incremental analysis of elasto-plastic beams and frames resting on an elastic half-plane. *J Eng Mech ASCE* 2019; 134(9): Article number 04017101, 1-9.

- [52] Tezzon E, Tullini N, Minghini M. Static analysis of shear flexible beams and frames in adhesive contact with an isotropic elastic half-plane using a coupled FE-BIE model. *Eng Struct* 2015; 104:32–50.
- [53] Tezzon E, Tullini N, Lanzoni L. A coupled FE-BIE model for the static analysis of Timoshenko beams bonded to an orthotropic elastic half-plane. *Eng Anal Bound Elem* 2016; 71:112–128.
- [54] Tullini N, Tralli A, Lanzoni L. Interfacial shear stress analysis of bar and thin film bonded to 2D elastic substrate using a coupled FE-BIE method. *Finite Elem Anal Des* 2012; 55:42–51.
- [55] Tezzon E, Tralli A, Tullini N. Debonding of FRP and thin films from an elastic half-plane using a coupled FE-BIE model. *Eng Anal Bound Elem* 2018; 93:21-28.
- [56] Tullini N, Tralli A, Baraldi D. Stability of slender beams and frames resting on 2D elastic half-space. *Arch Appl Mech* 2013; 83(3):467–482.
- [57] Tullini N, Tralli A, Baraldi D. Buckling of Timoshenko beams in frictionless contact with an elastic half-plane. *J Eng Mech* 2013; 139(7):824–831.
- [58] Narayanaswami R, Adelman HM. Inclusion of transverse shear deformation in finite element displacement formulations. *AIAA J* 1974; 12(11):1613–1614.
- [59] Reddy JN. On locking-free shear deformable beam finite elements. *Comput Meth Appl Mech Eng* 1997; 149(1-4):113–132.
- [60] Friedman Z, Kosmatka JB. An improved two-node Timoshenko beam finite element. *Comput Struct* 1993; 47(3):473–481.
- [61] Minghini F, Tullini N, Laudiero F. Locking-free finite elements for shear deformable orthotropic thin-walled beams. *Int J Numer Methods Eng* 2007; 72(7):808–834.
- [62] Stark RF. Integration of singularities in FE/BE analyses of soil-foundation interaction with non-homogeneous elastic soils. *Meccanica* 2001; 36(4):329-350.
- [63] Gurtin ME, Sternberg E. Theorems in linear elastostatics for exterior domains. *Arch Ration Mech Anal* 1961; 8:99–119.

- [64] Cowper GR. The shear coefficient in Timoshenko's beam theory. *J Appl Mech ASME* 1966; 33:335–340.
- [65] Erwin VJ, Stephan EP. Adaptive approximations for 3-D electrostatic plate problems. *Adv Eng Software* 1992; 15(3–4):211–215.
- [66] Graham IG, McLean W. Anisotropic mesh refinement: the conditioning of Galerkin boundary element matrices and simple preconditioners. *Journal on Numerical Analysis* 2006; 44(4): 1487–1513.
- [67] Whitman RV, Richart FE. Design Procedures for Dynamically Loaded Foundations. *J Soil Mech Foundations Div*, 1967; 93(6):169–193.

FIGURE CAPTIONS

Fig. 1. Beam with rectangular cross-section resting on an elastic half-space.

Fig. 2. Transverse beam displacements with uniform contact stress distribution (a) and contact stress underneath a rigid foundation (b).

Fig. 3. Beam on elastic half-space subdivided into equal FEs.

Fig. 4. Examples of discretizations of a contact surface subdivided with $n_x = 8$ elements and by varying n_y and $n_{x,end}$.

Fig. 5. Euler-Bernoulli beam loaded by a vertical point force P_z at midspan with $\alpha L = 5$ (a, c) and 25 (b, d). Vertical displacement (a, b) and surface pressures $r(x, 0)$ (c, d) along the beam length. Results obtained with the proposed model and $n_y = 1$ (dashed line), $n_y = 3$ (continuous line), $n_y = 5$ (solid dashed line), and results obtained with the 3D FEM (solid circles).

Fig. 6. Euler-Bernoulli beam loaded by a vertical point force P_z at midspan with $\alpha L = 5$ (a) and 25 (b). Surface tractions at midspan along the beam width for $n_y = 1$ (dashed line), $n_y = 3$ (continuous line), $n_y = 5$ (solid small dashed line).

Fig. 7. Euler-Bernoulli beam loaded by a vertical point force P_z at midspan with $\alpha L = 5$ (a, c) and 25 (b, d). Relative difference for $w(0)$ (a, b) and $r(0, 0)$ (c, d) versus n_x for the proposed model with $n_y = 1$ (dashed line), $n_y = 3$ (continuous line), $n_y = 5$ (solid dashed line), and for the 3D FEM (line with solid circles).

Fig. 8. One quarter of the 3D FEM of a beam on half-space, case with beam subdivided into 4 equal FEs.

Fig. 9. Euler-Bernoulli beam loaded by a vertical point force P_z at midspan with $\alpha L = 5$ (a, c) and 25 (b, d). Bending moment along the beam length (a, b) and relative difference for $M(0)$ versus the overall number of degrees of freedom (DOFs) (c, d). Results obtained with the proposed model and $n_y = 3$ (continuous line), and with the 3D FEM (line with solid circles).

Fig. 10. Beam loaded by a vertical point force P_z at midspan with $\alpha L = 1$ (a, c, e) and 5 (b, d, f). Dimensionless vertical displacement (a, b), surface traction $r(x, 0)$ (c, d) and bending moment (e, f) versus x/L for $\phi = 0$ (continuous line) and 0.3 (dashed line).

Fig. 11. Beam loaded by a vertical point force P_z at midspan with $\alpha L = 10$ (a, c, e) and 100 (b, d, f). Dimensionless vertical displacement (a, b), surface traction $r(x, 0)$ (c, d) and bending moment (e, f) versus x/L for $\phi = 0$ (continuous line) and 0.3 (dashed line). In (b) cross symbols refer to Boussinesq solution.

Fig. 12. Beam loaded by a vertical point force P_z at midspan. Vertical displacement at midpoint $w(0)$ and beam end $w(L/2)$ (a), traction $r(L/2 - 2L/n_x, 0)$ close to the beam end (b) versus αL for $\phi = 0$ (continuous line) and 0.3 (dashed line).

Fig. 13. Beam loaded by a vertical point force P_z at midspan. Bending moment at midspan versus αL for $\chi = L/b$ equal to 10, 30, 100 (continuous lines). Dashed lines represent Biot solution.

Fig. 14. Beam loaded by an uniform force distribution with $\alpha L = 1$ (a, c, e) and 5 (b, d, f). Dimensionless vertical displacement (a, b), surface traction (c, d) and bending moment (e, f) versus x/L for $\phi = 0$ (continuous line) and 0.3 (dashed line).

Fig. 15. Beam loaded by an uniform force distribution with $\alpha L = 10$ (a, c, e) and 100 (b, d, f). Dimensionless vertical displacement (a, b), surface traction (c, d) and bending moment (e, f) versus x/L for $\phi = 0$ (continuous line) and 0.3 (dashed line). In (b) cross symbols refer to Love solution.

Fig. 16. Beam loaded by an uniform force distribution. Vertical displacement at midpoint $w(0)$ and beam end $w(L/2)$ (a), traction $r(0, 0)$ (b) versus αL for $\phi = 0$ (continuous line) and 0.3 (dashed line). Large dashed line refers to traction obtained with $n_y = 1$ and $\phi = 0$.

Fig. 17. Beam loaded by a couple at midspan with $\alpha L = 1$ (a, c, e) and 5 (b, d, f). Dimensionless vertical displacement (a, b), surface traction (c, d) and bending moment (e, f) versus x/L for $\phi = 0$ (continuous line) and 0.3 (dashed line).

Fig. 18. Beam loaded by a couple at midspan with $\alpha L = 10$ (a, c, e) and 100 (b, d, f). Dimensionless vertical displacement (a, b), surface traction (c, d) and bending moment (e, f) versus x/L for $\phi = 0$ (continuous line) and 0.3 (dashed line).

TABLE CAPTIONS

Tab. 1. Reference results for a beam on elastic half-space subject to a vertical point force P_z at midspan, obtained with $n_x = 2^{10}$, $n_{x,end} = 3$ and a power-graded subdivision along y direction with $n_y = 7$ and $\beta = 3$.

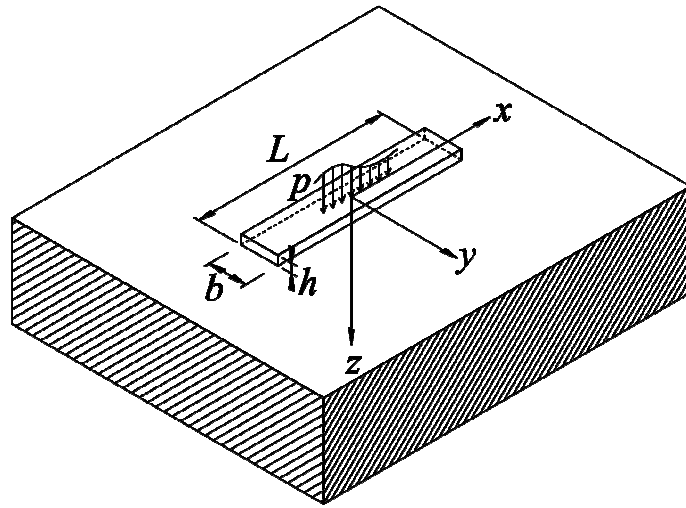


Fig. 2. Beam with rectangular cross-section resting on an elastic half-space.

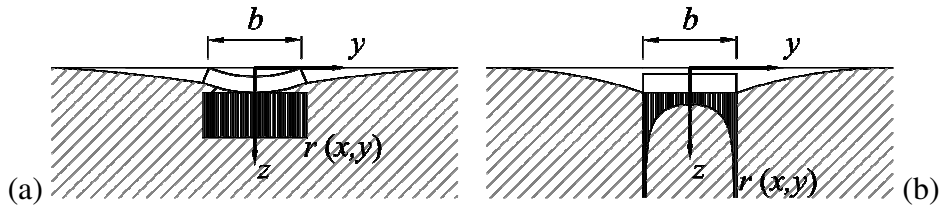


Fig. 2. Transverse beam displacements with uniform contact stress distribution (a) and contact stress underneath a rigid foundation (b).

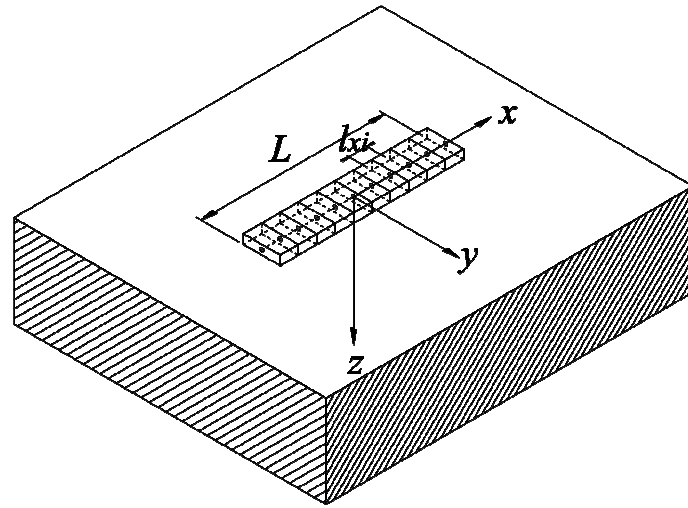


Fig. 3. Beam on elastic half-space subdivided into equal FEs.

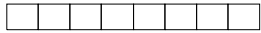
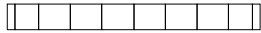
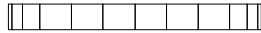



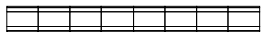
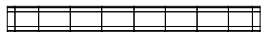
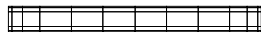
		$n_{x, end}$		
		1	2	3
n_y	1			
	3			
	5			

Fig. 4. Examples of discretizations of a contact surface subdivided with $n_x = 8$ elements and by varying n_y and $n_{x, end}$.

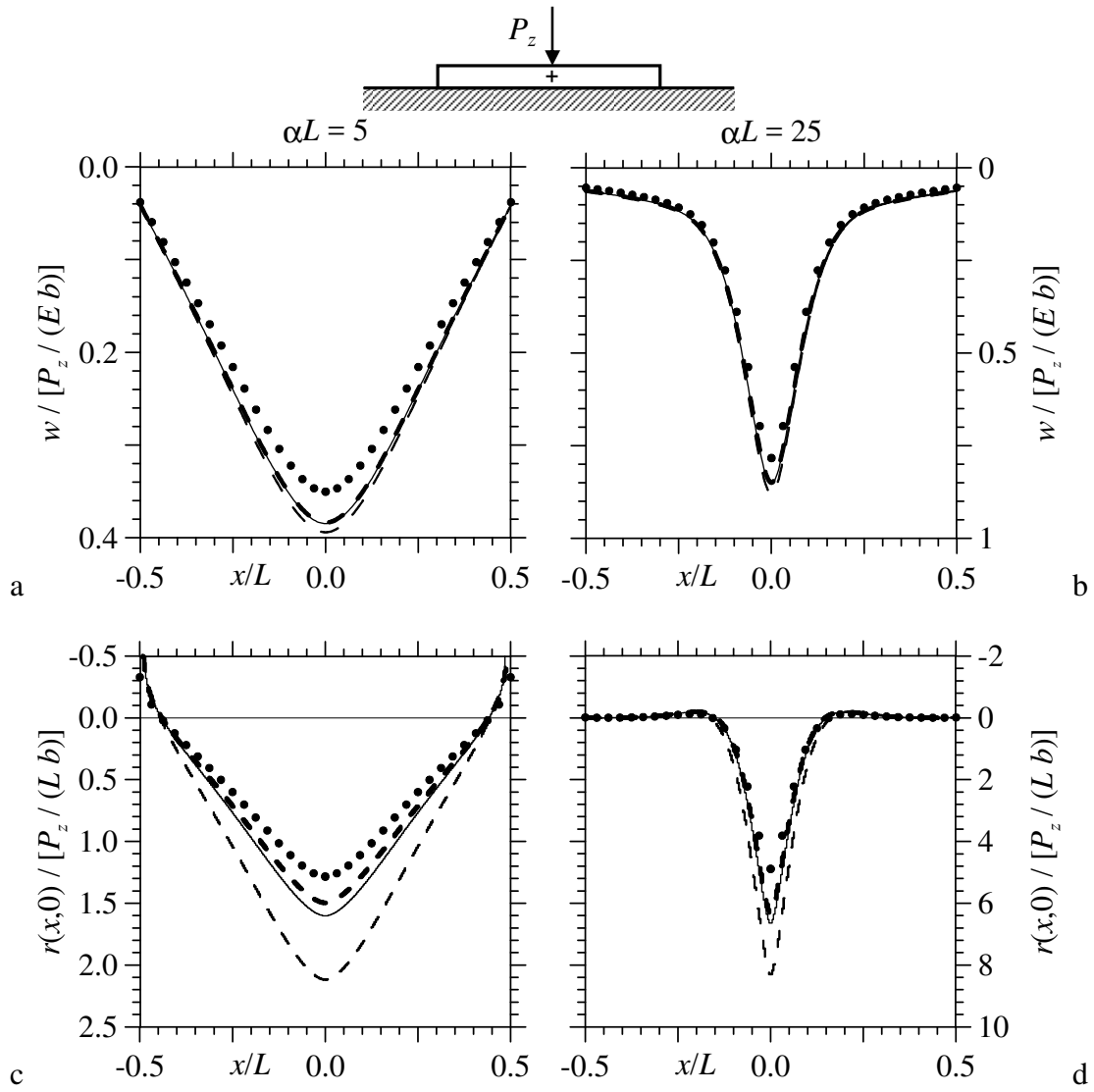


Fig. 5. Euler-Bernoulli beam loaded by a vertical point force P_z at midspan with $\alpha L=5$ (a, c) and 25 (b, d). Vertical displacement (a, b) and surface pressures $r(x, 0)$ (c, d) along the beam length. Results obtained with the proposed model and $n_y = 1$ (dashed line), $n_y = 3$ (continuous line), $n_y = 5$ (solid dashed line), and results obtained with the 3D FEM (solid circles).

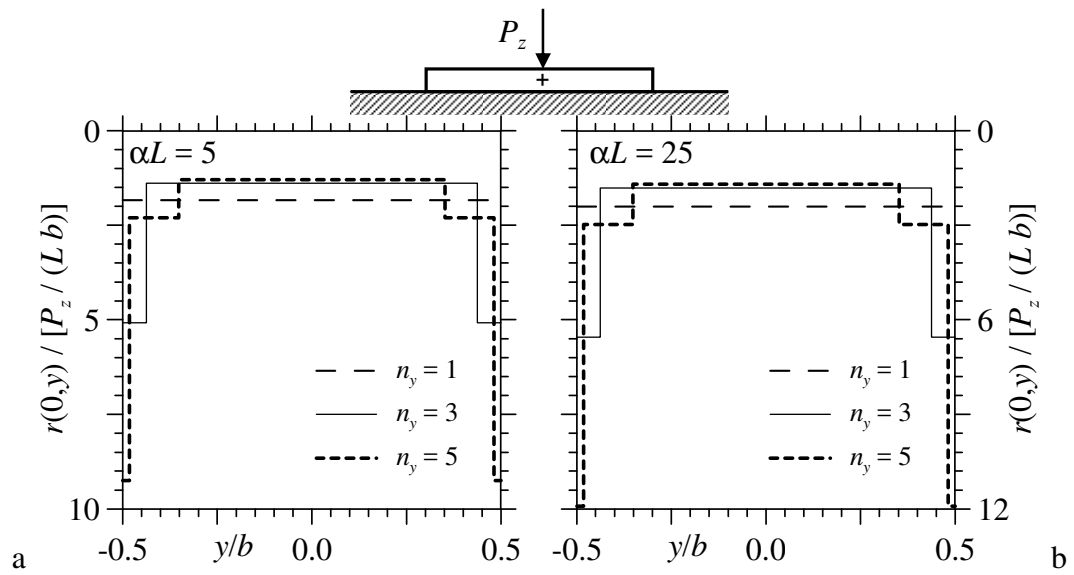


Fig. 6. Euler-Bernoulli beam loaded by a vertical point force P_z at midspan with $\alpha L = 5$ (a) and 25 (b). Surface tractions at midspan along the beam width for $n_y = 1$ (dashed line), $n_y = 3$ (continuous line), $n_y = 5$ (solid small dashed line).

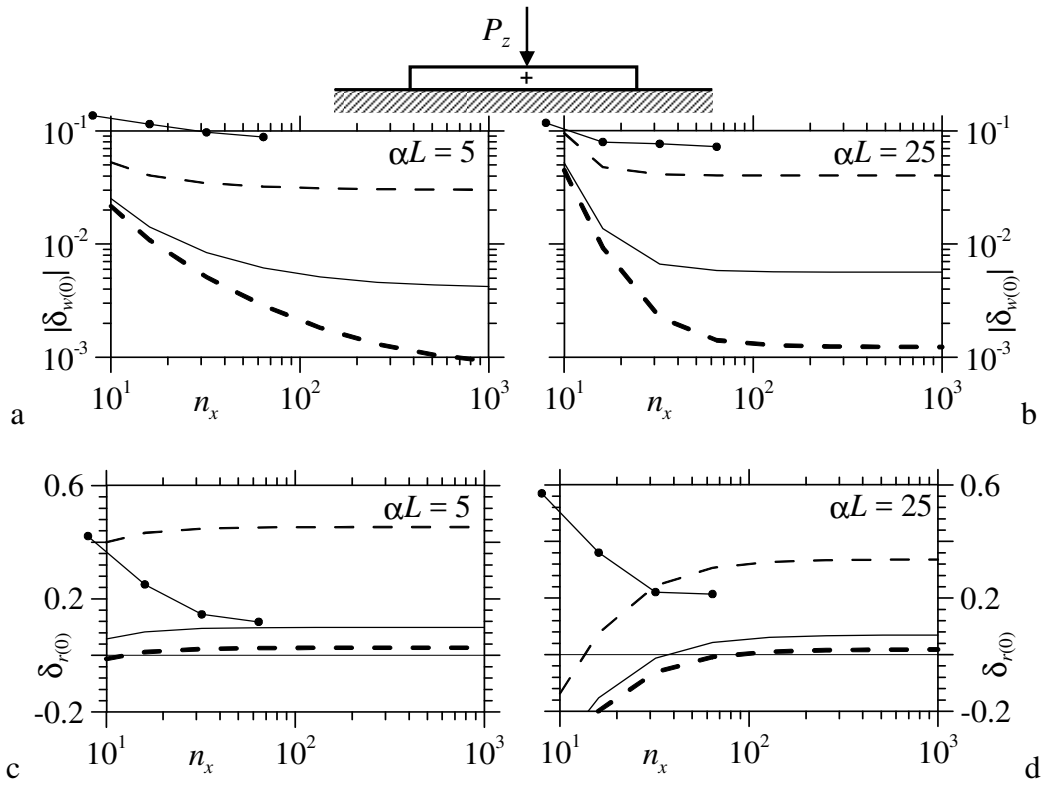


Fig. 7. Euler-Bernoulli beam loaded by a vertical point force P_z at midspan with $\alpha L = 5$ (a, c) and 25 (b, d). Relative difference for $w(0)$ (a, b) and $r(0, 0)$ (c, d) versus n_x for the proposed model with $n_y = 1$ (dashed line), $n_y = 3$ (continuous line), $n_y = 5$ (solid dashed line), and for the 3D FEM (line with solid circles).

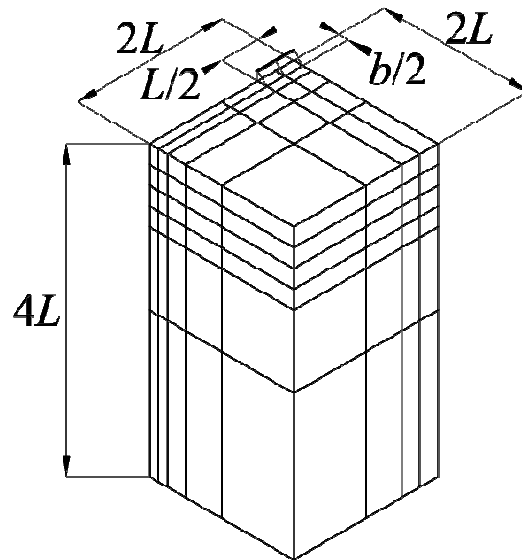


Fig. 8. One quarter of the 3D FEM of a beam on half-space, case with beam subdivided into 4 equal FEs.

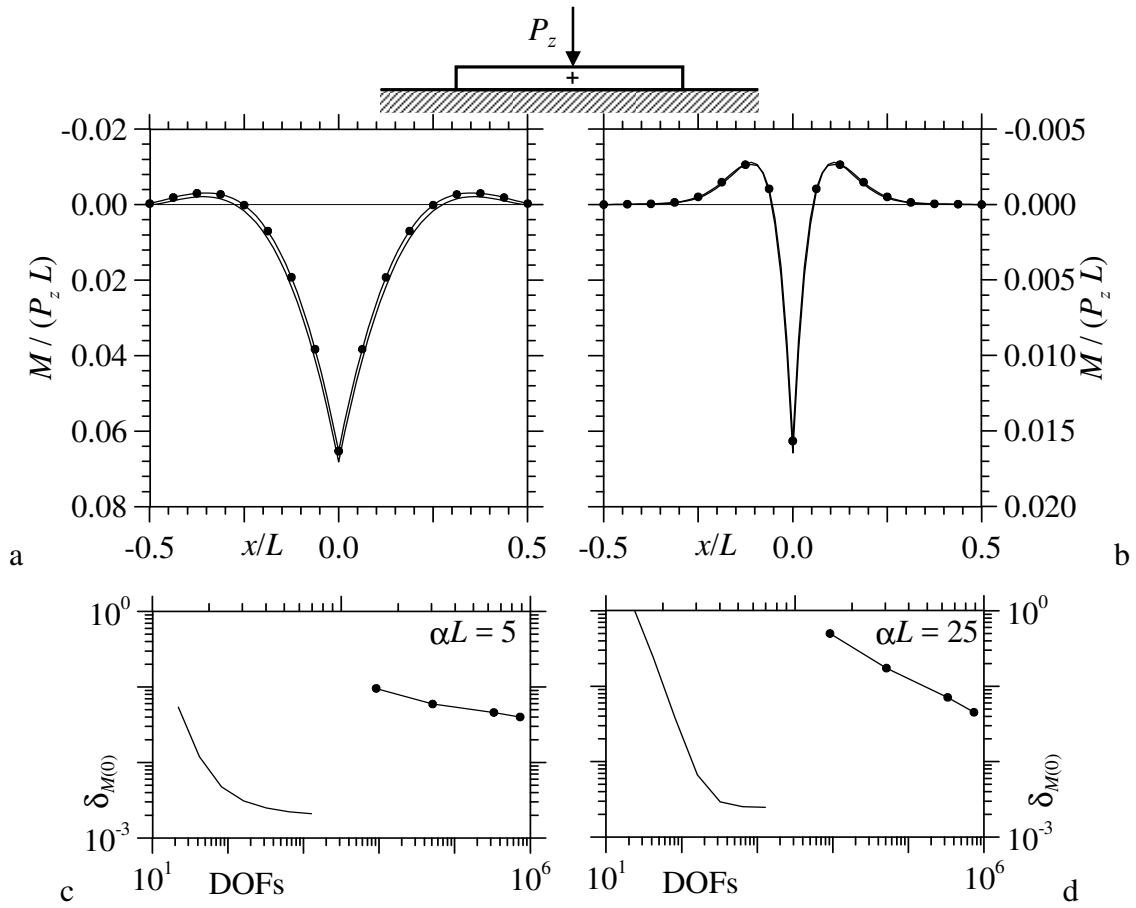


Fig. 9. Euler-Bernoulli beam loaded by a vertical point force P_z at midspan with $\alpha L = 5$ (a, c) and 25 (b, d). Bending moment along the beam length (a, b) and relative difference for $M(0)$ versus the overall number of degrees of freedom (DOFs) (c, d). Results obtained with the proposed model and $n_y = 3$ (continuous line), and with the 3D FEM (line with solid circles).

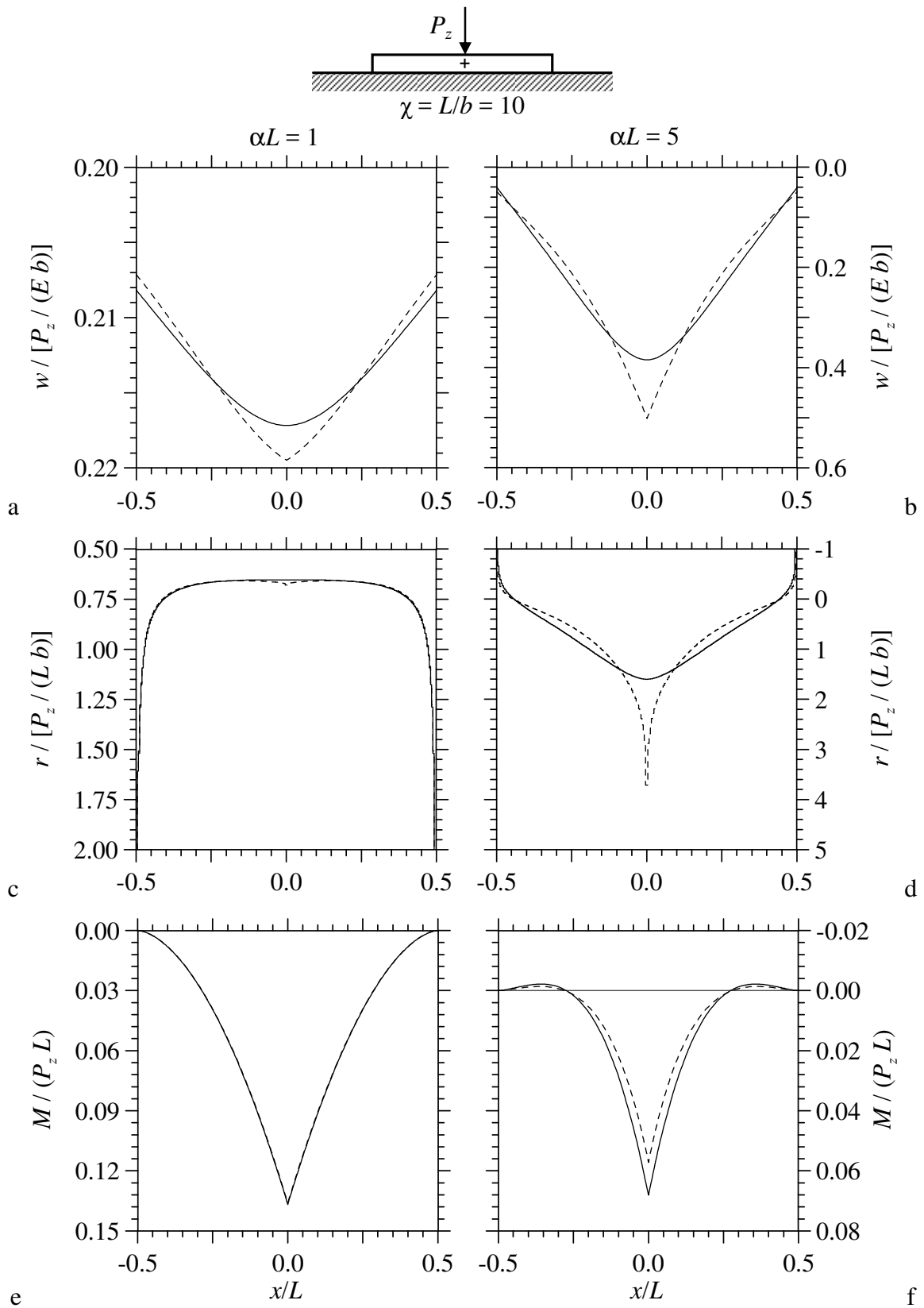


Fig. 10. Beam loaded by a vertical point force P_z at midspan with $\alpha L = 1$ (a, c, e) and 5 (b, d, f). Dimensionless vertical displacement (a, b), surface traction $r(x, 0)$ (c, d) and bending moment (e, f) versus x/L for $\phi = 0$ (continuous line) and 0.3 (dashed line).

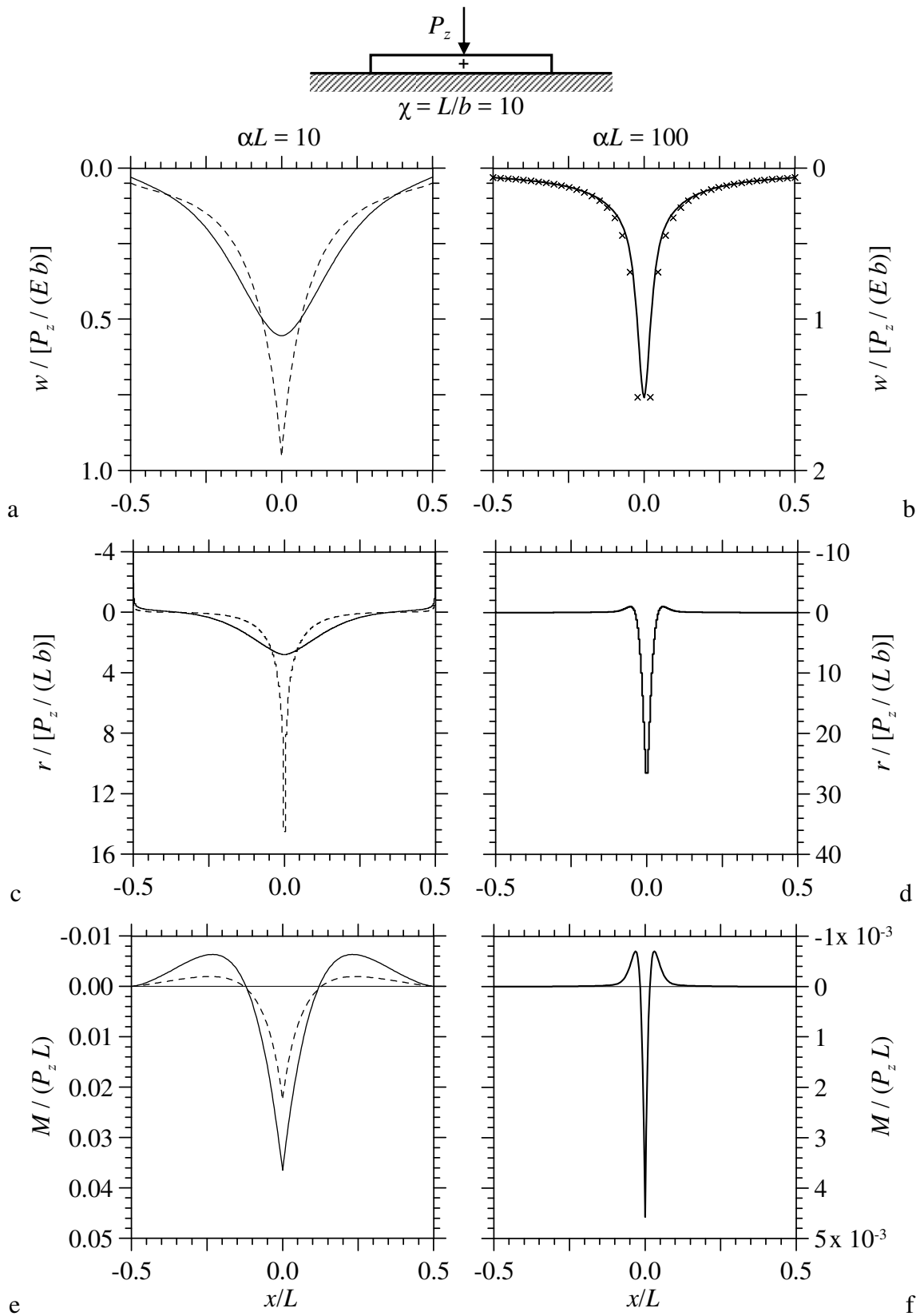


Fig. 11. Beam loaded by a vertical point force P_z at midspan with $\alpha L = 10$ (a, c, e) and 100 (b, d, f). Dimensionless vertical displacement (a, b), surface traction $r(x, 0)$ (c, d) and bending moment (e, f) versus x/L for $\phi = 0$ (continuous line) and 0.3 (dashed line). In (b) cross symbols refer to Boussinesq solution.

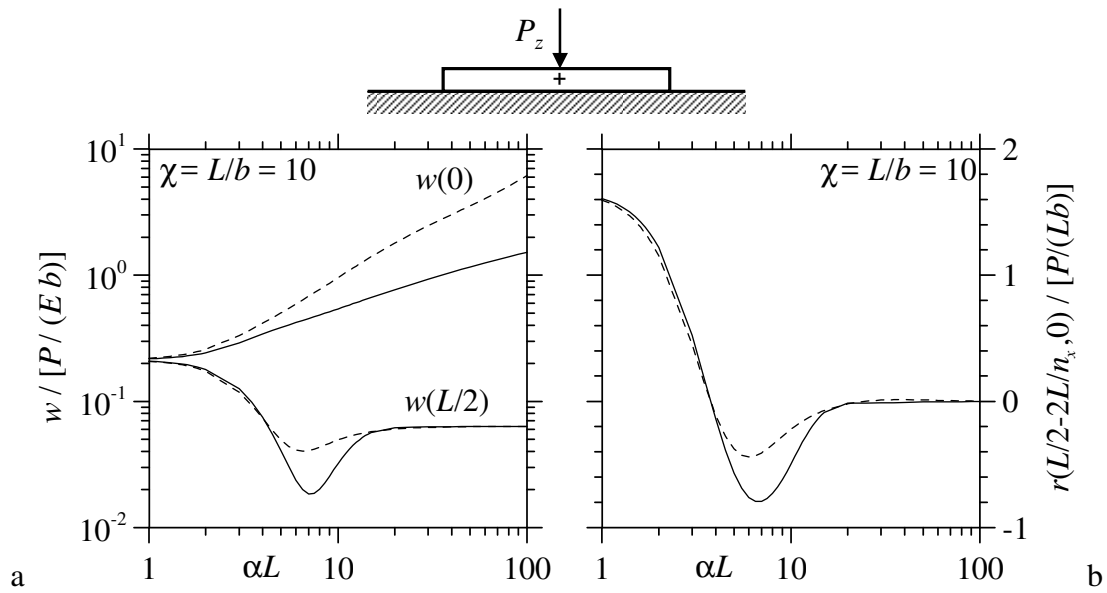


Fig. 12. Beam loaded by a vertical point force P_z at midspan. Vertical displacement at midpoint $w(0)$ and beam end $w(L/2)$ (a), traction $r(L/2 - 2L/n_x, 0)$ close to the beam end (b) versus αL for $\phi = 0$ (continuous line) and 0.3 (dashed line).

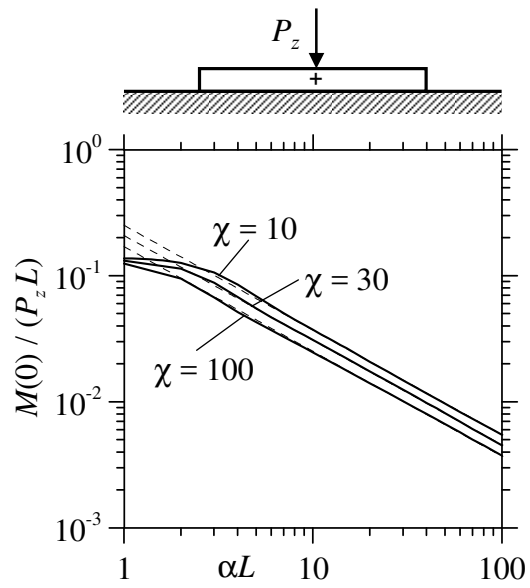


Fig. 13. Beam loaded by a vertical point force P_z at midspan. Bending moment at midspan versus αL for $\chi = L/b$ equal to 10, 30, 100 (continuous lines). Dashed lines represent Biot solution.

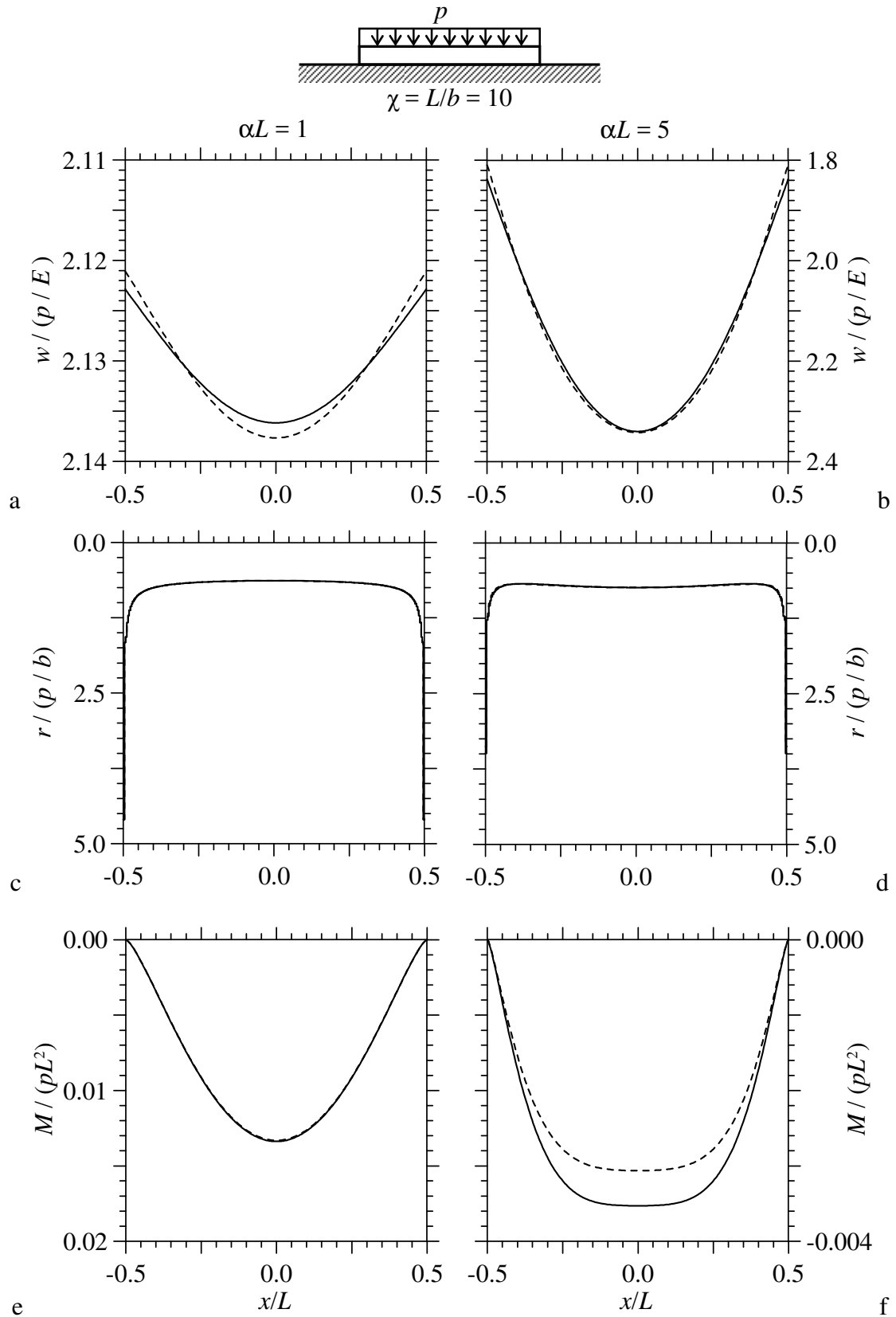


Fig. 14. Beam loaded by an uniform force distribution with $\alpha L = 1$ (a, c, e) and 5 (b, d, f). Dimensionless vertical displacement (a, b), surface traction (c, d) and bending moment (e, f) versus x/L for $\phi = 0$ (continuous line) and 0.3 (dashed line).

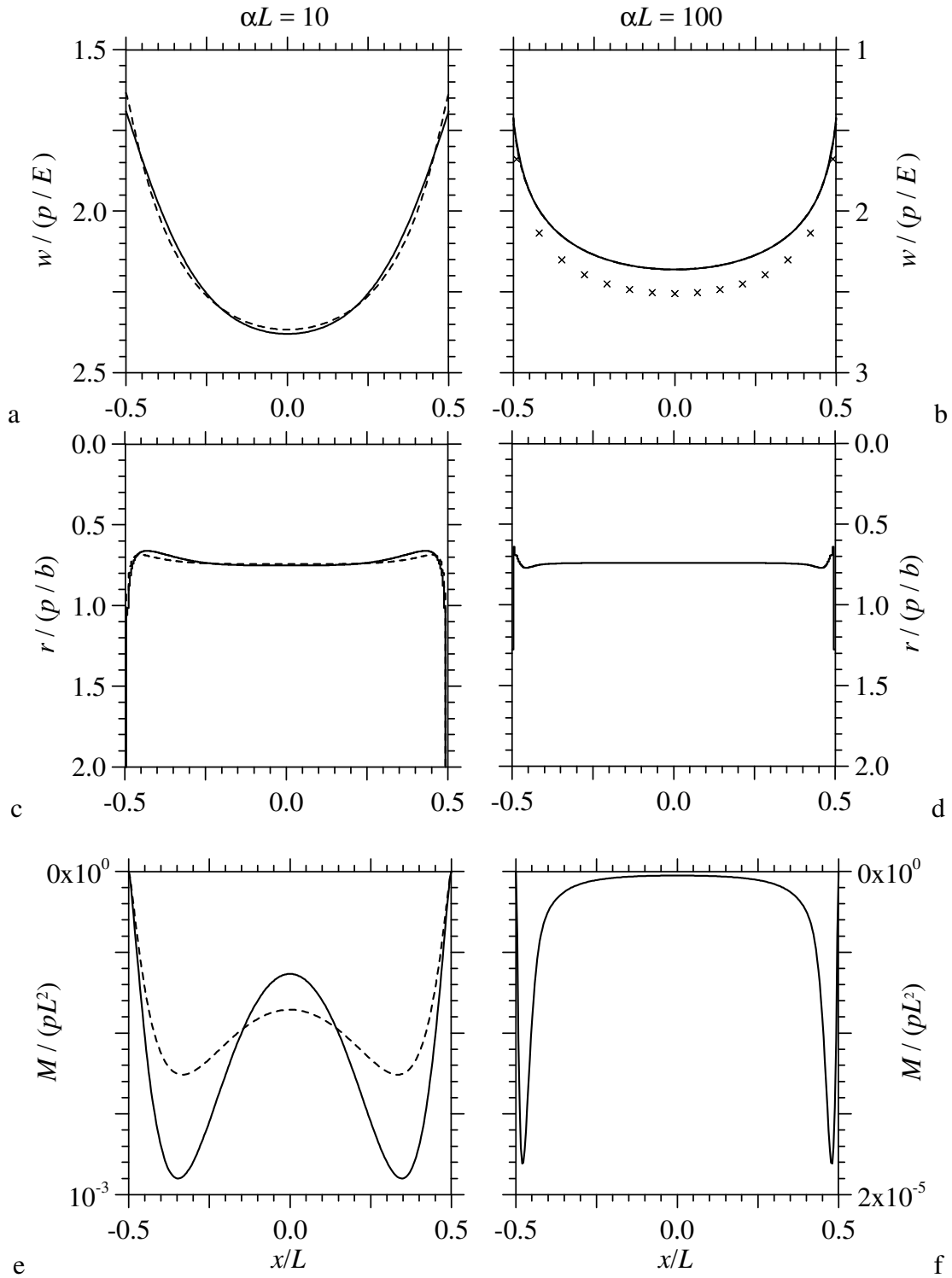
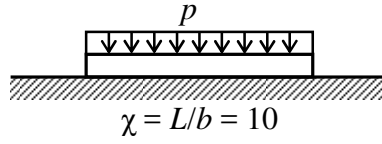


Fig. 15. Beam loaded by an uniform force distribution with $\alpha L = 10$ (a, c, e) and 100 (b, d, f).

Dimensionless vertical displacement (a, b), surface traction (c, d) and bending moment (e, f) versus x/L for $\phi = 0$ (continuous line) and 0.3 (dashed line). In (b) cross symbols refer to Love solution.

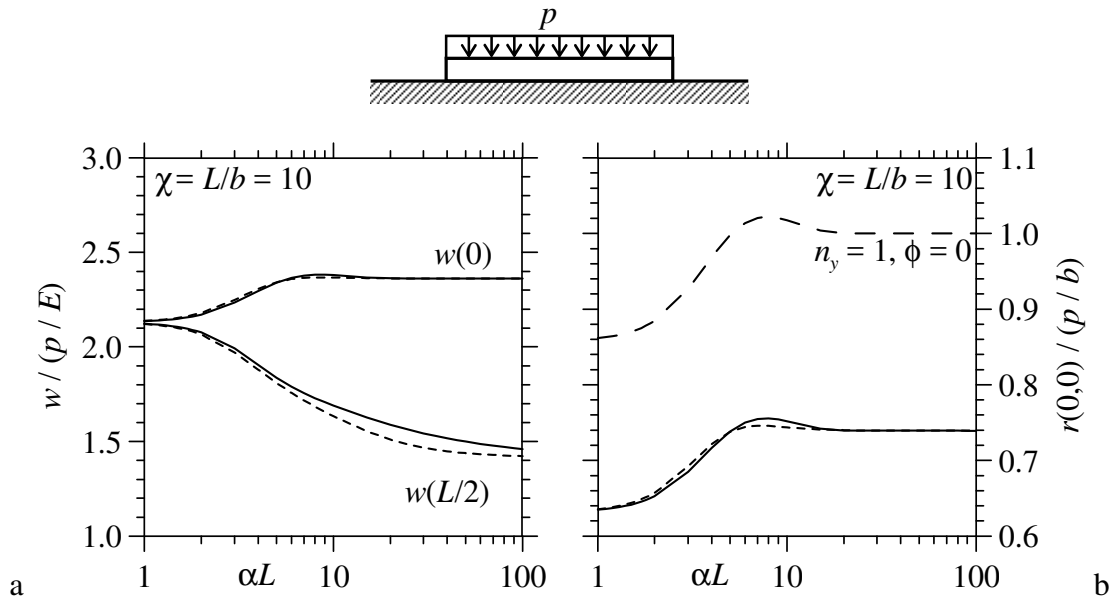


Fig. 16. Beam loaded by an uniform force distribution. Vertical displacement at midpoint $w(0)$ and beam end $w(L/2)$ (a), traction $r(0, 0)$ (b) versus αL for $\phi = 0$ (continuous line) and 0.3 (dashed line).

Large dashed line refers to traction obtained with $n_y = 1$ and $\phi = 0$.

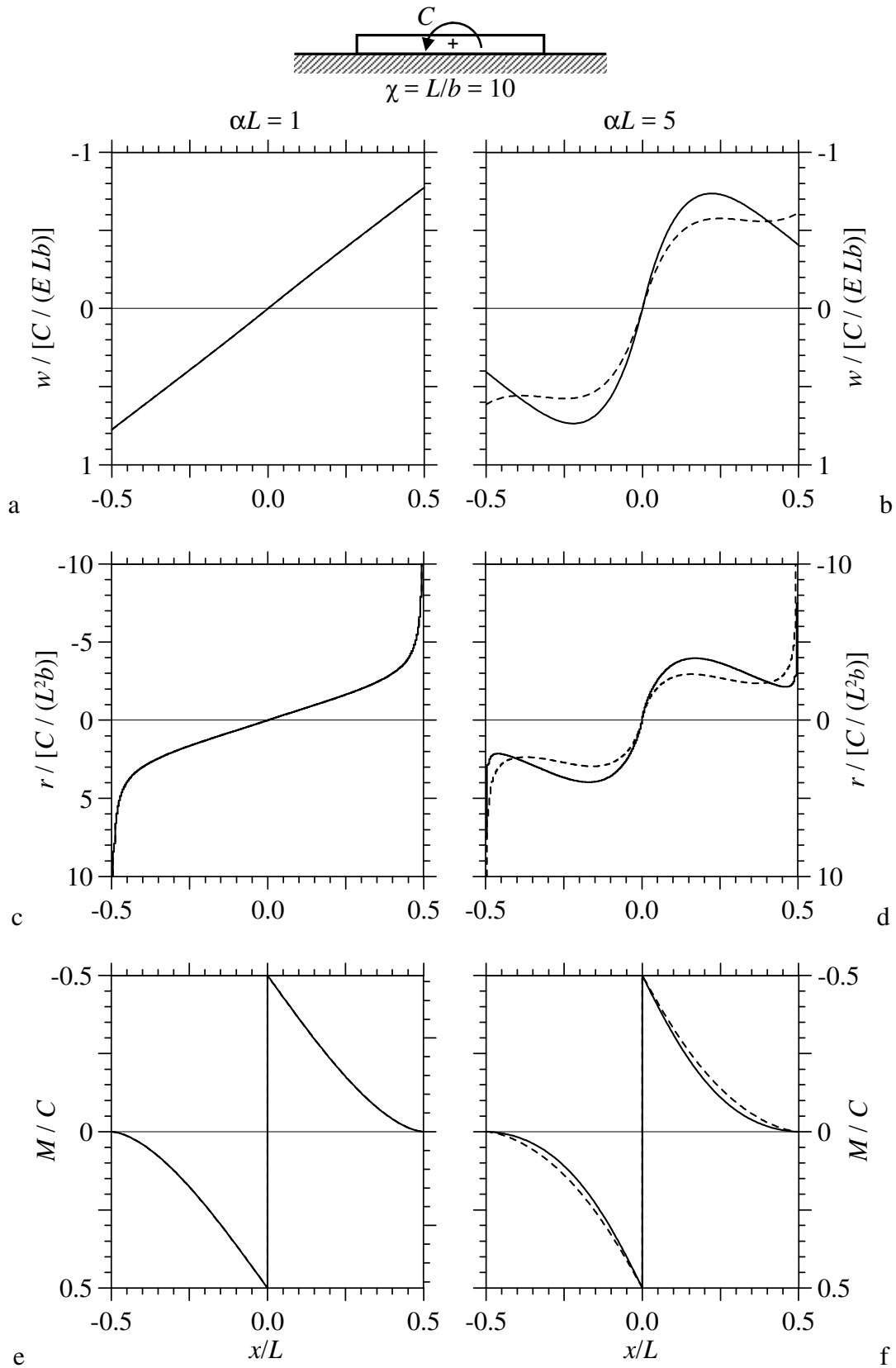


Fig. 17. Beam loaded by a couple at midspan with $\alpha L = 1$ (a, c, e) and 5 (b, d, f). Dimensionless vertical displacement (a, b), surface traction (c, d) and bending moment (e, f) versus x/L for $\phi = 0$ (continuous line) and 0.3 (dashed line).

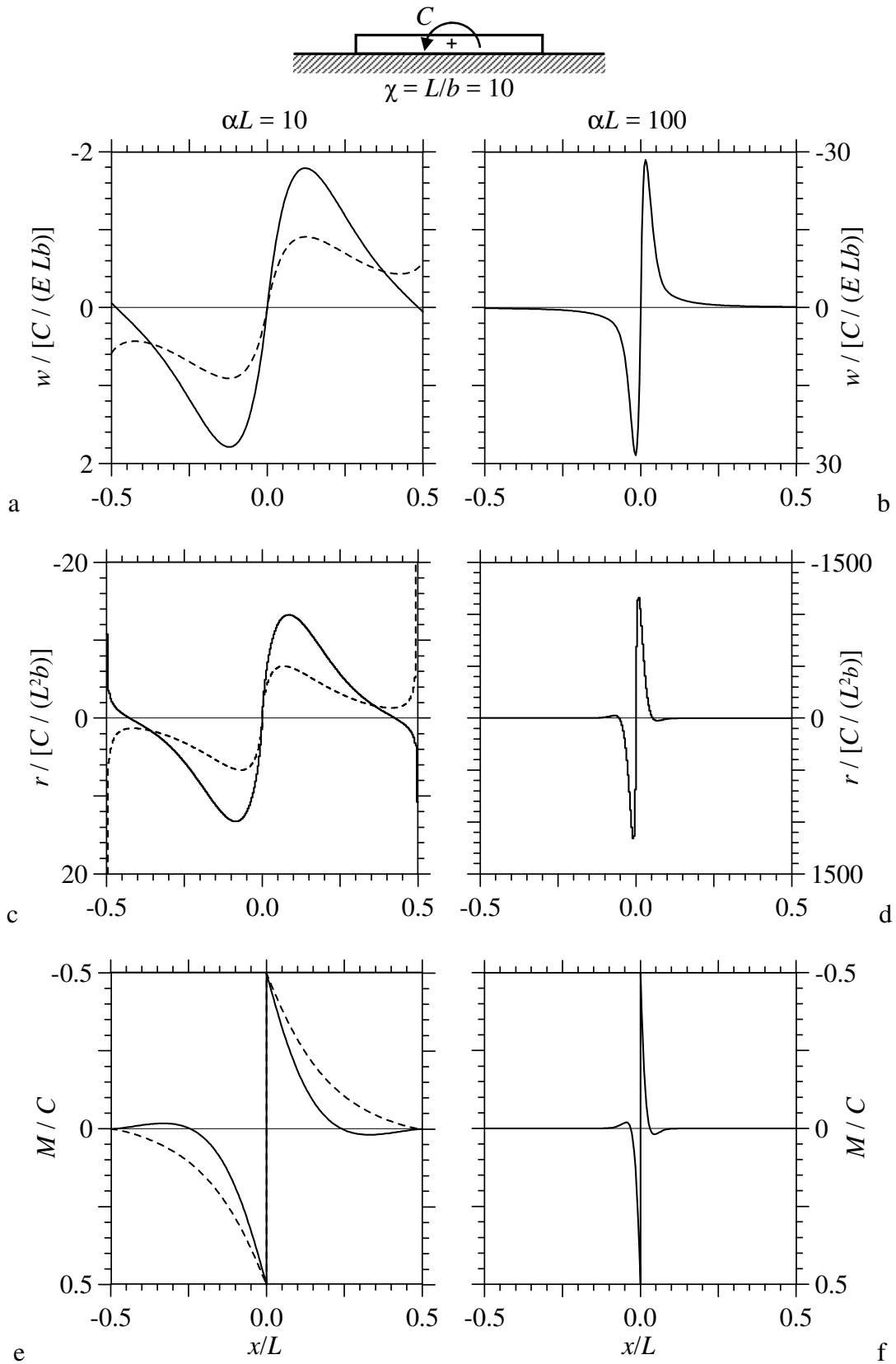


Fig. 18. Beam loaded by a couple at midspan with $\alpha L = 10$ (a, c, e) and 100 (b, d, f). Dimensionless vertical displacement (a, b), surface traction (c, d) and bending moment (e, f) versus x/L for $\phi = 0$ (continuous line) and 0.3 (dashed line).

		$w^{\text{REF}}(0)/[P_z / (E b)]$	$r^{\text{REF}}(0,0)/[P_z / (L b)]$	$M^{\text{REF}}(0)/(P_z L)$
αL	5	0.3833	1.4572	0.068005
	25	0.8485	6.2215	0.016388

Tab. 1. Reference results for a beam on elastic half-space subject to a vertical point force P_z at midspan, obtained with $n_x = 2^{10}$, $n_{x,end} = 3$ and a power-graded subdivision along y direction with $n_y = 7$ and $\beta = 3$.